EFFECT OF THE HOST ON CELLULAR THERAPIES FOR BONE HEALING

by

Laura Beth Meszaros

BS Biosystems and Agricultural Engineering, University of Kentucky, 2004

Submitted to the Graduate Faculty of

Swanson School of Engineering in partial fulfillment

of the requirements for the degree of

Doctor of Philosophy

University of Pittsburgh

2010

UNIVERSITY OF PITTSBURGH

SWANSON SCHOOL OF ENGINEERING

This dissertation was presented

by

Laura B Meszaros

It was defended on

November 19, 2010

and approved by

Gregory M Cooper PhD, Assistant Professor, Department of Surgery

Partha Roy PhD, Associate Professor, Department of Bioengineering

Charles Sfeir DDS, PhD, Associate Professor, Department of Oral Biology

Dissertation Director: Johnny Huard PhD, Professor, Department of Orthopaedic Surgery

EFFECT OF THE HOST ON CELLULAR THERAPIES FOR BONE HEALING

Laura Beth Meszaros, PhD

University of Pittsburgh, 2010

Muscle-derived stem cells (MDSCs) have been isolated from murine skeletal muscle and have the ability to differentiate into osteogenic, myogenic and chondrogenic lineages, among others. MDSCs may prove to be an attractive cell source for orthopaedic tissue engineering therapies. However, MDSCs must prove successful in many patient populations before clinical translation becomes a reality. MDSCs have been characterized and studied extensively based on attributes of the donor animal. To date, little is known about the effect of the host animal or surrounding tissue environment on MDSC therapies. These studies were undertaken to determine the efficacy of MDSCs in bone formation and bone healing in different hosts, representing different patient groups. MDSCs are known to exhibit sexual dimorphism, by donor sex, of osteogenic differentiation. Therefore, MDSC-mediated ectopic bone formation and cranial bone defect healing were compared between male and female host animals. Castrated male and ovariectomized female hosts were also examined in MDSC-mediated ectopic bone formation and cranial bone defect healing studies, in order to determine the role of host sex hormones in MDSC osteogenic therapies. Moreover, castrated males and ovariectomized females represent aged hosts, as these animals exhibit some aging symptoms related to loss of sex hormones. Lastly, MDSCs have only previously been applied to freshly created defects, so a delayed application study was carried out to determine if MDSCs could heal established defects. MDSCs were applied to a cranial defect, which had been previously created and allowed to fill with scar-like

fibrous tissue, to determine the efficacy of MDSCs in unfavorable bone defect environments or as treatment for non-unions. The results of these studies helped to elucidate the effect of host animal and tissue environment on MDSC-mediated bone tissue engineering therapies.

TABLE OF CONTENTS

LIST OF TABLES

LIST OF FIGURES

NOMENCLATURE

ANOVA – analysis of variance

BMP – bone morphogenetic protein

Cast – castrated male

CSD – critical size defect

EDTA – ethylenediaminetetraacetic acid

GFP – green fluorescent protein

HA – hydroxyapatite

MDSC – muscle-derived stem cell

MHC – myosin heavy chain

Ovx – ovariectomized female

PBS – phosphate buffered saline

PREFACE

I would first like to extend my gratitude to my mentor, Dr. Johnny Huard, who took a chance with a second-hand graduate student. You have taught me much about “telling the story”. You are never lacking in persistence, energy or enthusiasm for new ideas, and I hope I still have these qualities when I reach your current standing in my own career.

I would also like to thank the members of my dissertation committee, Dr. Greg Cooper, Dr. Partha Roy, and Dr. Charles Sfeir. I greatly appreciate your time and guidance in my dissertation research. Moreover, to Dr. Greg Cooper, thank you for your confidence in my future career and for always asking me, “Then what?”

Thank you to all members of the Huard Lab and SCRC, both present and past, who have helped me along the way. Most importantly, thank you to Dr. Arvydas Usas for many, many hours of his time for surgery and microCT scanning. Also, I am indebted to students Zach Nelson and Matt Huard for their many hours of microtome sectioning. Thank you to administration and technical staff of the SCRC, including Dr. Burhan Gharaibeh, Michelle Witt, Jessica Tebbets, Jim Cummins, Matt Bosco, Michele Keller, and Jennifer Holliman, all of whom kept the lab moving in the right direction. I also extend my greatest thanks to Drs. Karin Payne and Julie Phillippi, not only for their friendship and guidance, but also for their example as female researchers.

“We have been friends together, In sunshine and in shade” - Caroline E. S. Norton And indeed, graduate school has given us all our share of sunshine and shade. Thank you to Allison Bean, Diana Gaitan, Jess LoSurdo, Joost Wagenaar, Melanie Ruffner, Noah Papas, Paul Enders, Shelly Gabriele, and Silvia Wognum for your support as we forged our way through graduate school together.

Two special teachers, Susie Carter and Linda McClung, have shaped my life and career choices. Their overwhelming dedication to the science education of their students has touched thousands of lives, including mine. Principles I learned through science fair projects are still applicable in my research today. I also never see wildflowers without fond remembrance.

Lastly, and most importantly, I would like to thank my family. Your unwavering confidence in me and my abilities has been a great comfort in times of frustration or doubt. I know that I would not be here today without you.

1.0 INTRODUCTION

1.1 MUSCLE-DERIVED STEM CELLS

1.1.1 MDSC Isolation and Characterization

Muscle-derived stem cells (MDSCs) have been isolated from mouse skeletal muscle using a modified preplate technique [1-4]. Briefly, this technique involves enzymatically dissociating cells from a muscle biopsy and then separating MDSCs based on adhesion characteristics in collagen coated flasks. After two hours pp1 (preplate 1) is established, and the medium containing non-adherent cells is transferred to a new flask. At consequent 24 hour intervals, media are transferred to new flasks and pp2 through pp6 are established. After cultivation for 1-2 weeks, pp6 cells proliferate and form colonies, and these cells are termed MDSCs. MDSCs have been well-characterized by our research group. Populations or clones of MDSCs have been shown to express measurable levels of desmin, CD34, Flk-1, Sca-1, and MyoD and do not express C-kit or CD45 [2, 3]. MDSCs have been shown to be multipotent, differentiating into musculoskeletal tissues such as bone, cartilage, and skeletal muscle, in addition to endothelial, neural and hematopoietic tissues [3-9].

1.1.2 Muscle-Derived Cells and Bone Formation

Cells from murine skeletal muscle, including MDSCs, have been shown to differentiate toward an osteogenic lineage in vitro and form bone in vivo when in the presence of either BMP2 or BMP4. In an early study, it was shown that MDSCs treated with BMP2 become osteogenic, shown by increased ALP activity and expression of osteocalcin, and non-myogenic, through decreased expression of desmin and lack of formation of myotubes in vitro [3]. MDSCs transduced with an adenovirus encoding for BMP2 produce ectopic bone when implanted in skeletal muscle, and the MDSCs are localized to bone tissue formed and express osteocalcin. Non-purified muscle cells when transduced can also deliver BMP2, but these cells do not differentiate into osteoblasts. MDSCs transduced with an adenovirus to produce BMP2 can also heal critical sized cranial defects [3]. Additionally, when compared to an immortalized osteogenic cell line, pp6 cells were similar in terms of BMP2 responsiveness and ectopic bone production after transduction with adenovirus encoding for BMP2, proving superior to other primary cells (bone marrow stromal cells, chondrocytes and skin fibroblasts) [10]. MDSCs can undergo osteogenic differentiation with BMP4 treatment in vitro, and retrovirally transduced cells can produce high amounts of BMP4. These BMP4 transduced cells can then produce ectopic bone in skeletal muscle, as well as improve bone healing in critical sized cranial defects [8, 9, 11]. Muscle-derived cells from rats, when retrovirally transduced for BMP4, can also heal critical sized segmental femoral defects [12].

Human skeletal muscles cells isolated in a similar manner to MDSCs (up to pp5) respond to BMP2 by increasing ALP activity, a marker of osteogenic differentiation. Human muscle-derived cells can also produce BMP2 when transduced with retrovirus, and these transduced cells produce ectopic bone in immunocompromised mice [13]. Human muscle-derived cells

transduced with BMP2 heal critical size defects, and these human cells participate in healing by delivering BMP2, but a small fraction of human cells also differentiate into osteoblasts [14].

Several studies have investigated murine MDSCs transduced to produce proteins other than BMP2 and BMP4. MDSCs can also be retrovirally transduced to produce a BMP antagonist, Noggin. When MDSCs expressing both BMP4 and Noggin are used, the ratio of cells is important, and a dose dependent inhibition of bone formation by BMP4 expressing MDSCs is exhibited. Also, complete inhibition of ectopic bone formation with demineralized bone matrix implantation is observed when MDSCs expressing Noggin were used, and reduction of bone formation in a post-trauma heterotopic ossification model is seen [15]. Co-implantation of MDSCs retrovirally transduced with BMP4 and cells transduced with Noggin allows controlled in vivo bone growth in a critical sized cranial defect [16].

Angiogenesis and bone formation are intimately related, and MDSCs expressing BMP4, VEGF, and sFlt (a VEGF antagonist) have been investigated. When cells expressing VEGF and BMP4 are implanted in vivo, there is a synergistic effect on bone formation; furthermore, the ratio of VEGF to BMP4 is critical. When MDSCs express sFlt, this inhibits bone formation induced by BMP4 expressing cells [7]. BMP2 has similar synergistic effects with VEGF, and sFlt also inhibits bone formation by BMP2 expressing MDSCs [17].

1.1.3 Sex Differences in MDSCs

MDSCs are known to exhibit sex differences in muscle regeneration, as well as chondrogenic and osteogenic differentiation both in vivo and in vitro [18-20]. MDSCs isolated from female mice have higher regeneration efficiency when transplanted into mdx or mdx/SCID mice, a dystrophin deficient animal model of muscular dystrophy. In mdx mice, a significant effect of

host sex was also seen, with female hosts exhibiting higher regeneration [19]. Male MDSCs show superior chondrogenic differentiation in a micromass culture system in vitro and are also better at repairing a created osteochondral defect [20].

With regards to in vitro osteogenic differentiation after application of BMP4, MDSCs isolated from males have been proven superior. Male MDSCs show more differentiation, as measured through markers of osteogenic differentiation including staining for alkaline phosphatase (ALP), ALP activity, ALP and Runx2 gene expression. When MDSCs are single cell sorted and permitted to form colonies, more male MDSCs form colonies with high ALP expression. When MDSCs are treated with BMP4 and cultured in micromass, higher mineralization is observed in male MDSCs, another indication of in vitro differentiation. Lastly, in vivo implantation of MDSCs of both sexes showed that male MDSCs produce denser and more consistent volumes of ectopic bone, while female MDSCs produce variable volumes of ectopic bone. A trend of host sex dependence was also observed with in vivo bone formation, with male hosts showing more bone formation, although this was not significant [18].

1.2 SEXUAL DIMORPHISM IN STEM CELL THERAPIES AND DISEASE

In addition to MDSCs, other progenitor or stem cells also exhibit sexual dimorphism, by donor sex, of differentiation potential. Bone marrow stem cells from human females do not decrease their differentiation potential with advanced age of donor, but this does occur with bone marrow stem cells from human males [21]. Endothelial progenitor cells from male donors are less migrative and form fewer colonies [22]. Bone marrow stem cells from female donors are more effective at functionally repairing cardiac ischemia than the same cells from male donors [23].

Osteoprogenitors derived from female rat bone increase proliferation and differentiation in response to progesterone, while the same cells from male rats do not [24]. Adipose stem cells (ASCs) isolated from donors of different sexes also exhibit divergent differentiation potential. In separate studies, male rabbit ASCs are more osteogenic than those from female donors, while female mouse ASCs are more adipogenic [25, 26].

It is well known that male and female humans have different skeletal size and bone mass, with males being larger and possessing higher bone mass [27, 28]. However, other more subtle differences in orthopaedic disease are currently being examined. In fact, osteoarthritis, osteoporosis and fractures are more common in women [29]. Differences in body growth and development can contribute to these conditions, as well as muscle, tendon and ligament injuries [29]. Because women have, on average, a longer lifespan than men, disabilities and disease affecting elderly populations occur more often in women [30].

When faced with an aging population, sexually dimorphic prevalence of diseases, and sex differences in cellular progenitor therapies to treat these diseases, it will become increasingly important to consider sex of patient when choosing treatments. Currently, outcomes of transplantation, whether solid organ or bone marrow are known to be affected by sex of donor and sex mismatch between donor and host [31]. Future stem cell therapies should include gender considerations in order to maximize positive outcomes.

1.3 BONE BIOLOGY AND FRACTURE HEALING

1.3.1 Bone Biology

Bone tissue consists three types of cells: osteoblasts, osteoclasts and osteocytes, and these cells are surrounded by a matrix consisting of type I collagen and other peptides (osteocalcin, osteopontin, BMPs), as well as an inorganic component of hydroxyapatite [32]. Osteoblasts are bone forming cells that are derived from mesenchymal stem cells (MSCs) when they are stimulated with specific growth factors. Osteoblasts become active in the presence of parathyroid hormone and produce bone matrix and contribute to mineralization of that matrix [32]. Osteocytes are osteoblasts that are fully surrounded by bone and are connected through canaliculi [32]. Osteoclasts are derived from macrophages and are involved in bone resorption. Bone formation and resorption through the actions of osteoblasts and osteoclasts is a coupled process and is tightly regulated [32]. Coupled formation and resorption occurs constantly in response to hormones and mechanical signals [33]. The three tissues that make up mature bone are fatty hematopoietic marrow, bone tissue and periosteum. Structure of bone can be classified based on maturity (woven vs lamellar bone) or organization (cortical vs cancellous bone). Woven bone is a relatively weak, disorganized bone tissue with rapid turnover; it forms during embryonic development and fracture repair and is replaced by a less active, more organized lamellar bone [33]. Cortical bone makes up outer surfaces and is denser, stronger than the trabecular structure of cancellous bone which makes up the interior of bones and has higher turnover [32].

1.3.2 Endochondral Ossification

Endochondral ossification, also known as enchondral ossification, is the process by which mesenchymal progenitor cells transition to chondrocytes and later bone cells (osteocytes, osteoblasts, and osteoclasts) [34, 35]. This process occurs in a developing embryo limb buds, long bone growth plates, and long bone fracture healing (described below), as well as in some in vivo bone formation research models. First, mesenchymal cells proliferate, condense and transition to a chondroprogenitor phenotype, followed by differentiation of these chondroprogenitors to hypertrophic chondrocytes [35]. In developing embryo limb buds and pre-adult growth plates , mesenchymal cells are mesenchyme derived, but in fracture healing or bone formation research models, these cells can be from more distant tissues like bone marrow, muscle, trabecular bone, dermis, adipose, periosteum, pericyte, blood, synovial membrane, articular cartilage, placenta, or cord blood sources [35]. Vascular interactions with chondrocytes then bring about differentiation of osteoblasts and osteoclasts from these mesenchymal cells, which in turn, produce and remodel bone matrix [34].

1.3.3 Long Bone Fracture Healing

Fracture healing follows a well-defined sequence of inflammation, bone formation, and bone remodeling [32, 33]. When a fracture occurs, not only is the bone damaged, but soft tissues and blood vessels surrounding the bone are also affected, and a hematoma results at the fracture site. Necrotic tissue can also result from damage and cause inflammatory processes to occur. Organization of the hematoma is usually considered the first step of repair of a fracture, and disruption of this hematoma can adversely affect healing [33]. Vascularization is also very

important to healing, and disruption either through surgical removal of periosteal or intramedullary blood supplies is also considered detrimental to healing [33]. Growth factors released by the hematoma and surrounding injured tissues control the subsequent healing process. MSCs migrate to the fracture site through blood vessels or from injured tissue and form a callus. This callus consists of cartilage, fibrous tissue and woven bone, and it surrounds the fracture site, stabilizing and providing a framework for repair. The outer portion known as the hard callus consists of bone formed through intramembranous ossification, and the inner portion is the soft callus made of cartilage and fibrous tissue [33]. Gradually, through endochondral ossification, the soft callus is replaced with woven bone until the fracture is stabilized and the opposing ends are bridged [32, 33]. Remodeling, through the coupled action of osteoblasts and osteoclasts, replaces the disorganized woven bone with organized bone resembling the pre-fracture structure. Remodeling processes can continue for years following fracture repair [33]. There are two types of fracture union: clinical union, when the site is painless and stable, and radiographic union, which occurs following clinical union and is marked by radiographic evidence of bone crossing the fracture line [33].

Motion and mechanical strains at the fracture site are important for healing and treatment. If no movement is allowed to occur at the fracture site and opposing sides are closely approximated, repair can occur through creeping substitution where migrating osteoclasts followed by osteoblasts move from one side of the fracture to the other [32]. This type of healing occurs without callus formation and is also known as primary bone healing [33]. Methods of treatment with restricted movement such as cast immobilization and external fixation allow bone healing through callus formation, while internal fixation of fractures can actually be detrimental because complete immobility does not allow callus formation, and forces are supported through

the fixation devices rather than the bone, resulting in decreased healing [32, 33]. Intramedullary devices allow restricted motion and callus formation occurs during healing [32].

1.3.4 Long Bone Non-unions

Failure in fracture healing can be classified as either delayed union or non-union. A non-union is classified by the FDA “when a minimum of 9 months has elapsed since injury and the fracture shows no visible progressive signs of healing for 3 months” [36]. However, the distinction between delayed union and non-union is arbitrary, and there is not a consensus definition among clinicians, although most rely on some radiological analysis of healing [37].

Non-unions can be classified as either hypertrophic (large callus with incomplete bridging) or atrophic (little to no callus formation with bone resorption) [32, 33]. There are many variables related to the injury, patient, tissue and treatment which can all contribute to non-union. Injury-related issues are open fractures (soft tissue and vascular damage, infection), comminuted fractures (disruption of soft tissue), intra-articular fractures (movement of the joint), segmental fractures (distal end of segmental fractures has diminished blood supply), soft tissue interposition, and damage to blood supply (injury or surgical procedure) [33, 34, 38]. Patient variables include old age, poor nutrition, altered hormonal status, and use of nicotine, corticosteroids, or chemotherapeutics [33, 34, 38]. Tissue variables are type of bone (cortical bone heals slower than cancellous), bone necrosis, and disease or infection within the bone [33, 34]. Treatment variables consist of restoration of fragment apposition, loading and micromotion (both are considered to increase healing) and fracture stabilization [33, 34]. Disruption of the early hematoma can also contribute to a non-union [33].

1.3.5 Craniofacial Bone Defects

Craniofacial surgeons face bone tissue deficits in several situations: either as the primary problem (cleft palate) or as a consequence of surgical procedures (craniosynostosis) [39]. Maxillofacial surgeons can also deal with bone defects due to skeletal hypoplasia, either in the mandible or other sites, which are often treated with distraction osteogenesis techniques [39].

1.4 CURRENT BIOLOGIC TREATMENTS

Biologic treatments for bony defects, whether these defects are caused by insufficient long bone repair or surgical removal of bone in craniofacial repairs, are clinically available. Autograft or allograft bone tissue can be used, but each has positive and negative attributes that must be considered. Autologous iliac crest bone graft, which is osteogenic, osteoconductive, and osteoinductive, is considered the gold standard to which other biologic treatments are compared, but donor site morbidity is a major concern and available tissue is limited [40, 41]. Allograft bone does not have limitations of availability; however, disease transmission and immune reactions are a concern, and the allograft must be treated which may diminish its utility [41, 42]. Another treatment is application of demineralized bone matrix, which is produced by chemical treatment of allograft bone and contains collagen I and osteoinductive proteins [41, 42]. Osteoinductive proteins such as human BMPs (rhBMP2 and rhBMP7) are currently used clinically, as well as combinations of demineralized bone matrix and BMPs [41-49]. Autologous bone marrow aspirate and platelet-rich plasma can also be applied to non-unions with some success; however, limited amounts of both are available from a patient [41, 42, 50]. Ceramics

like tricalcium phosphate and hydroxyapatite can provide an osteoconductive scaffold for a non-union [41, 42].

1.5 ANIMAL MODELS OF BONE FORMATION AND HEALING

1.5.1 Intramuscular Ectopic Bone Formation

Following Urist's preeminent 1965 manuscript "Bone: Formation by Autoinduction" [51], in vivo intramuscular ectopic (also termed heterotopic) bone formation assays have become the standard for determining the value of potential bone regeneration therapies. Work by our group has focused on virally transduced cells on gelatin scaffolds [52-54], but other studies have examined cell-free scaffolds [55], cells on hard scaffolds [56], or viral injection[57, 58] placed in muscle to produce ectopic bone.

1.5.2 Critical Size Cranial Defect Healing

Standardization of bone healing models (and the criteria used to define them) has been attempted by many researchers. A standard non-healing bone defect is needed for comparisons of efficacy of bone healing therapies. The concept of a critical size defect (CSD) was first established by Schmitz and Hollinger as "the smallest size intraosseous wound in a particular bone and species of animal that will not heal spontaneously during the lifetime of the animal" [59]. This definition was later modified to "a defect which has less than 10 percent bony regeneration during the lifetime of the animal" and fibrous connective tissue filling the defect is also mentioned as an

analog to a fibrous long bone nonunion [60]. CSD size in various species (rats, rabbits, cats, dogs, pigs, nonhuman primates, horses, guinea pigs) and locations (calvaria, mandible, long bones) has also been discussed [60]. Other subsequent definitions have changed duration of non-healing from “lifetime of the animal” to “duration of the study” [61]. Most recently, it has been proposed to do away with the term “critical size defect” as it has been previously defined for several reasons: “duration of the study” is non-standardized and based on each specific study, “lifetime of the animal” is unreasonable when making comparisons to lifespan of human patients, and lastly the fibrous tissue filling these defects is intimately positioned with the dura (and brain) in small animal models and treatments prohibiting debridement, which would mimic the clinical procedures of debridement of atrophic nonunion followed by placement of bone repair treatments [62].

For this work, a model of mouse calvarial bone repair was used. Our previous work shows that this defect, in the size and manner created, will not heal completely without intervention [7, 9, 14, 17, 63]. Therefore, this model of murine calvarial defect is used for comparison of efficacy of bone defect treatments in this work.

1.6 CASTRATION AND OVARIECTOMY AS MODELS OF AGING

Ovariectomy and castration are used often as animal models of aging. Both menopause and andropause are conditions encompassing all body systems which are linked to decreased sex hormone production related to aging. For research purposes, surgical removal of sex hormone producing organs (ovaries and testes, respectively) is a more time efficient method of modeling disease and aging processes related to sex hormones than data collected from aged mice.

Ovariectomy as a model of disease and aging has been used in many systems including neuroimmunomodulation, renal disease, stroke, and cardiac disease [64-67]. Likewise, castration has also been studied as a model of aging in blood pressure-related renal disease, neurobiology and thyroid disease [68-70].

While ovariectomy is a widely accepted model of postmenopausal osteoporosis [71, 72], ovariectomy is also used to test tissue engineered bone defect treatments, as well as mechanical and dietary effects on bone remodeling [73-75]. Castration is also used in studies of bone remodeling in the context of factors such as parathyroid hormone, RANKL and oxidative stress [76-78].

1.7 SIGNIFICANCE

MDSCs are an attractive option for future stem cell based therapies in many tissues, including bone. While MDSCs have been proven osteogenic both in vivo and in vitro, many questions remain before translation to clinical applications can occur. In order for clinical therapies to be successful, they must be able to be used in many patient populations. The goal of this work is to examine the osteogenic capacity of MDSCs in different hosts, each representing different patient groups. MDSCs are known to exhibit donor sex based differences in myogenic, chondrogenic, and osteogenic differentiation; therefore, differences in osteogenic capacity of MDSCs in both male and female hosts will be examined. Osteogenesis in ovariectomized and castrated hosts will also be studied; the rationale for this is two-fold: first, the role of sex hormones in MDSC-mediated osteogenesis can be elucidated, and second, ovariectomy and castration model age-related changes in sex hormone status and can provide insight into the role of MDSCs in aged

hosts. Finally, MDSCs will be examined in a non-healing bone defect filled with fibrous tissue to determine the utility of MDSCs in treating non-unions or defects in unfavorable host environments.

1.8 AIMS AND HYPOTHESES

1.8.1 Specific Aim 1: To determine the effect of host animal sex and sex hormones on bone formation mediated by MDSCs

Hypothesis: More MDSC-mediated intramuscular ectopic bone formation will occur in male than in female host animals. Castration and ovariectomy will not affect MDSC-mediated bone formation sex differences.

1.8.2 Specific Aim 2: To determine the effect of host animal sex and sex hormones on bone healing mediated by MDSCs

Hypothesis: MDSC-mediated cranial defect healing will be superior in male compared to female host animals. Castration and ovariectomy will not affect MDSC-mediated bone healing sex differences.

1.8.3 Specific Aim 3: To determine the effect of MDSCs when applied to an established non-healing bone defect

Hypothesis: MDSCs, when applied to a fibrous tissue filled non-healing bone defect, will induce healing in a manner similar to MDSCs applied at the time of creation of the defect.

2.0 EFFECT OF HOST SEX ON ECTOPIC BONE FORMATION MEDIATED BY MDSCS

2.1 INTRODUCTION

This study examined the effect of host sex and sex hormones on bone formation in mice. Using muscle-derived stem cells and an intramuscular ectopic bone formation model, hosts of four groups (unaltered male, castrated male, unaltered female and ovariectomized female) were evaluated using microCT analysis and histological staining. The hypotheses of this study were as follows: more MDSC-mediated intramuscular ectopic bone formation will occur in male than in female host animals, and castration and ovariectomy will not affect MDSC-mediated bone formation sex differences.

2.2 METHODS

2.2.1 MDSC Isolation and Retroviral Transduction

Muscle-derived stem cells (MDSCs) were isolated using the following technique, which both Qu-Petersen et al, 2002 and Gharaibeh et al, 2008 described in depth [1, 4]. Briefly, skeletal muscle from both lower limbs of a male C57BL/6J mouse was dissected, and connective and adipose tissues were removed. Following fine mincing, successive enzymatic digestions with

collagenase (Sigma-Aldrich), dispase (Invitrogen) and trypsin (Invitrogen) were performed. Finally, a single cell suspension was achieved by passing a mixture of cell digest and proliferation medium through 18G, 23G and 27G needles. Proliferation medium consists of the following: high glucose Dulbecco's modified Eagle medium (Invitrogen), 10% fetal bovine serum (Invitrogen), 10% horse serum (Invitrogen), .5% chick embryo extract (Accurate Chemical Co) and 1% penicillin-streptomycin (Invitrogen). This cell suspension was then plated onto collagen coated flasks. After two hours, non-adherent cells were transferred from the previous flask to a new collagen coated flask. After twenty-four hours, and every twenty-four hours following for 5 total days, this procedure of transferring non-adherent cells to a new collagen coated flask is repeated. Each step (and the cells resulting from it) are numbered pp1, pp2, pp3 …pp6 and the isolation procedure is termed "the preplate technique" [4]. Another nomenclature is RAC (rapidly adhering cells) for cells from the first two steps and first two hours of the isolation procedure and SAC (slowly adhering cells) for the cells from the latter steps and days two though five [1]. In this aim, the cells resulting from this isolation procedure will be called MDSCs.

Based on previous development of retroviral vectors in our laboratory, a retrovirus called CLB2/4G, encoding for both BMP4 and GFP, was applied to MDSCs in a 1:1 ratio with proliferation medium with 8 μg/mL of polybrene for 24 hours [11, 79]. These retrovirally transduced cells were then sorted using FACS (fluorescence activated cell sorting) and only cells expressing GFP (and therefore only cells expressing BMP4) were used in consequent experiments. These cells will be called MDSC-B4 in this aim. Average BMP4 secretion of MDSC-B4 was determined to be 168 ng/mL by 10^6 cells in 24 hours via human BMP4 ELISA (R&D Systems).

MDSCs were cultured in proliferation media and kept at low confluency until sufficient numbers were reached for experiments. Stocks of transduced MDSCs were also frozen at low passage number so all experiments could be performed using similar cells. Frozen stocks were stored in freezing media consisting of proliferation media and 10% dimethyl sulfoxide.

2.2.2 Surgical Procedure

For ectopic bone formation assays, four host animal groups were used: unaltered male, castrated male, unaltered female, and ovariectomized female C57BL/10J mice. All animals were purchased from Jackson Laboratories, and castration and ovariectomy were performed prior to acquisition at age 5 weeks. Surgeries were performed at age 12 weeks. After sacrifice, castration or ovariectomy were visually confirmed.

One day prior to implantation, 250,000 MDSC-B4 were placed on a 5mm by 5mm by 1mm gelatin sponge and allowed to adsorb onto the surface. Proliferation media was then added to cover the sponge, and the sponges were the cultured overnight until implantation.

Following sterile surgical procedures outlined in the University of Pittsburgh IACUC Protocol #0807916, each animal was anesthetized and bilateral incisions were made in the skin on the back of the hind limbs. A small pocket was made between the muscles and the gelatin sponge with MDSC-B4 was inserted. The incisions were then closed with sutures, and the animals were allowed to resume normal activity. Animals were euthanized at 21 and 42 days post implantation.

2.2.3 microCT Analysis

Ectopic bone formation was evaluated in all groups with a microCT scanner (VivaCT40, Scanco Medical) at 7, 14, 21, 28, 35, and 42 days post implantation. Mice were anesthetized and positioned prone in an animal scanning bed with the legs fixed in a specially designed holder. Scanning was performed with the following settings: energy of 55 kVp, intensity of 145 μA, nominal resolution of 35 μm, and integration time of 200 ms. Two-dimensional image slices were obtained and contour lines were drawn to define volume of interest (VOI). An appropriate threshold was chosen for the bone voxels by visually matching thresholded areas to grayscale images. The threshold was kept constant throughout the analyses. This led to a three-dimensional reconstruction of the ectopic bone and provided quantitative data on bone volume (mm3).

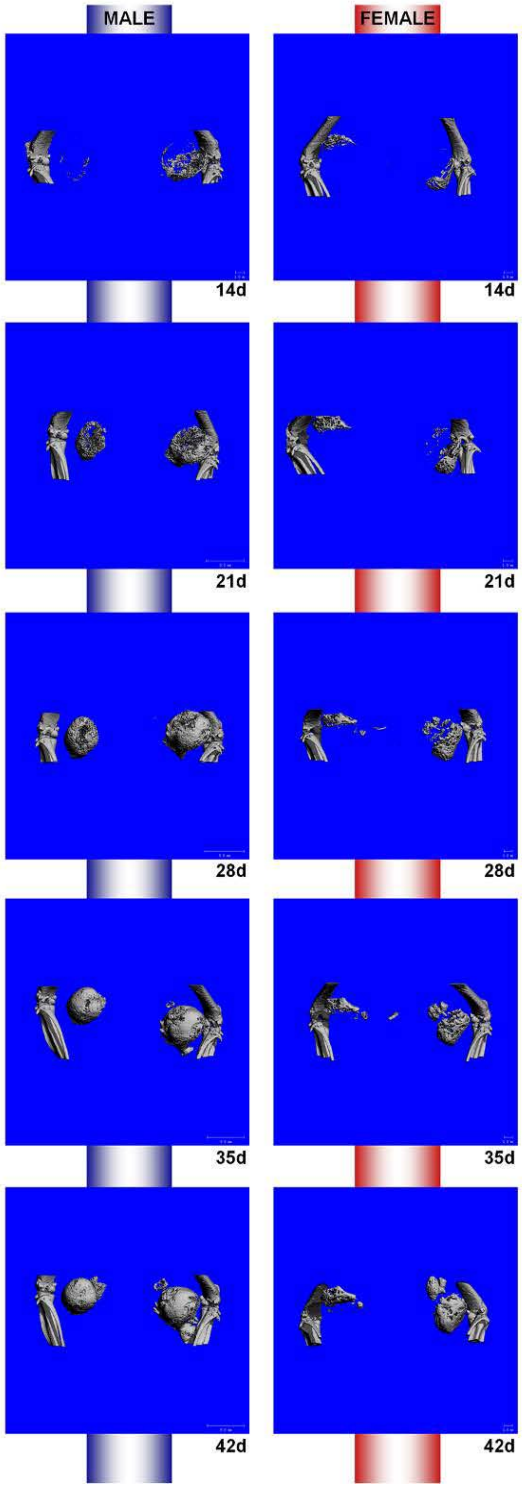

Figure 1. Representative microCT reconstructions of ectopic bone in male and female hosts

2.2.4 Histological Analysis

Following euthanasia, the ectopic bone and surrounding muscle tissue was dissected and placed in formalin (3.7% neutral buffered formaldehyde) for 24 hours. The samples were then decalcified in 10% EDTA (Sigma-Aldrich). Dehydration and then paraffin embedding followed, and samples were cut into 5 micron sections and dried.

Following deparaffinization and rehydration, sections of ectopic bone tissue were stained using standard procedures for hematoxylin and eosin staining (H&E) to determine general tissue morphology and Alcian blue staining for cartilage matrix. Donor cells were distinguished from host cells by staining for GFP, since all donor cells produced both GFP and BMP4. Briefly, after blocking in both 3% H_2O_2 in methanol and 2% horse serum in PBS, biotintylated anti-GFP antibody (Vector Laboratories) was applied at a 1:1000 dilution. Then, streptavidin/HRP (R&D) was applied at a 1:50 dilution followed by DAB Peroxidase Substrate Kit (Vector Laboratories) per manufacturer's instructions. Hematoxylin QS (Vector Laboratories) was used as a counterstain. Resultant stain showed donor cells expressing GFP (MDSC-B4) as brown and all cells from the host as purple.

Non-implanted hindlimb muscle from the four host groups was also examined histologically for both muscle fiber type distribution and blood vessel quantification. Fluorescent staining for fast and slow isoforms of myosin heavy chain was performed using anti-slow myosin heavy chain (Sigma) at 1:200 dilution and anti-fast myosin heavy chain (Sigma) at 1:200 dilution in conjunction with a MOM IgG Blocking Kit (Vector Laboratories) and appropriate secondary antibodies. CD31 staining for blood vessels was performed with anti-CD31 primary antibody (BD) at 1:100 dilution and appropriate secondary antibody. All fluorescent stained slides were also stained with DAPI to visualize all nuclei.

All images were taken on Nikon Eclipse E800 microscope equipped with a Retiga EXi digital camera using QCapture (brightfield images) or Northern Eclipse (fluorescent images) software.

2.2.5 Statistical Analysis

Sample size of 14-16 ectopic bone nodules per host group were used for volume and rate analysis. Fiber type distribution and vascularity were assessed on 4 hindlimb muscles per host group, with 10 random pictures from each muscle used to quantify measures. Bone volume (mm^3), fiber type distribution (number of slow fibers/ total number of fibers), vascularity (vessels/ total number of nuclei) are reported as mean ± standard deviation. Using SPSS statistical software, two-way repeated measures ANOVA with Tukey's post hoc analysis is used for volume and rate while one-way ANOVA with Tukey's post hoc analysis is used for fiber type distribution and vascularity measurements.

2.3 RESULTS

2.3.1 Volume

MDSC-mediated ectopic bone formation in four host groups (male, cast, female and ovx) was monitored with weekly microCT scanning, and the results are shown in Figure 2. In summary, male hosts (whether unaltered males or castrated males) form more bone than female hosts

(whether unaltered females or ovariectomized hosts) at 21, 28, 35 and 42 days post implantation of MDSC-B4 infused gelatin sponges. However, the volume of bone formed was not different between male and castrated hosts or between female and ovariectomized hosts.

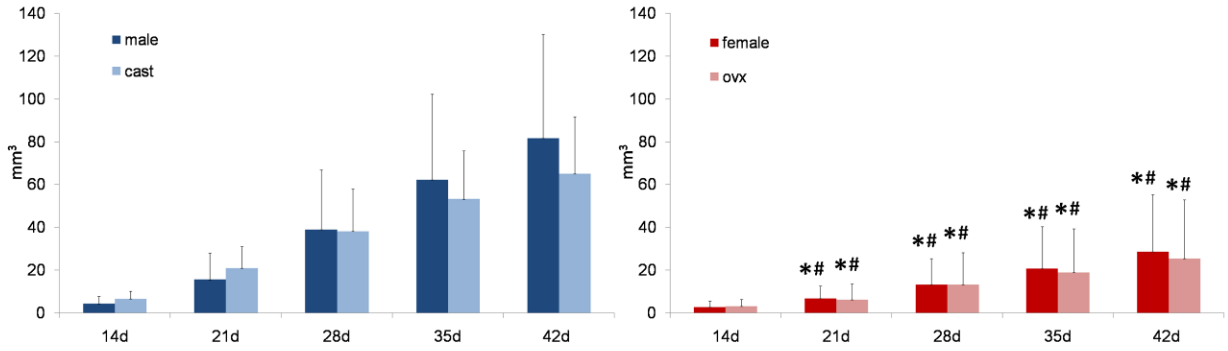

Figure 2. Volume (mm^3) of ectopic bone formed

Average ectopic bone volume formed (in mm^3) in male, castrated, female and ovariectomized groups. * indicates significantly different ($p<.05$) from male hosts at the same time point, and # indicates significantly different ($p>.05$) from cast hosts.

2.3.2 Rate

Rate of ectopic bone formation was also analyzed and summarized in Figure 3. As in volume analysis, male and castrated hosts showed no differences in bone formation rate. No differences were observed in bone formation rate between female and ovariectomized hosts either. However, the rate of bone formation in both female and ovariectomized hosts was significantly slower than ectopic bone formation rate in male and castrated hosts.

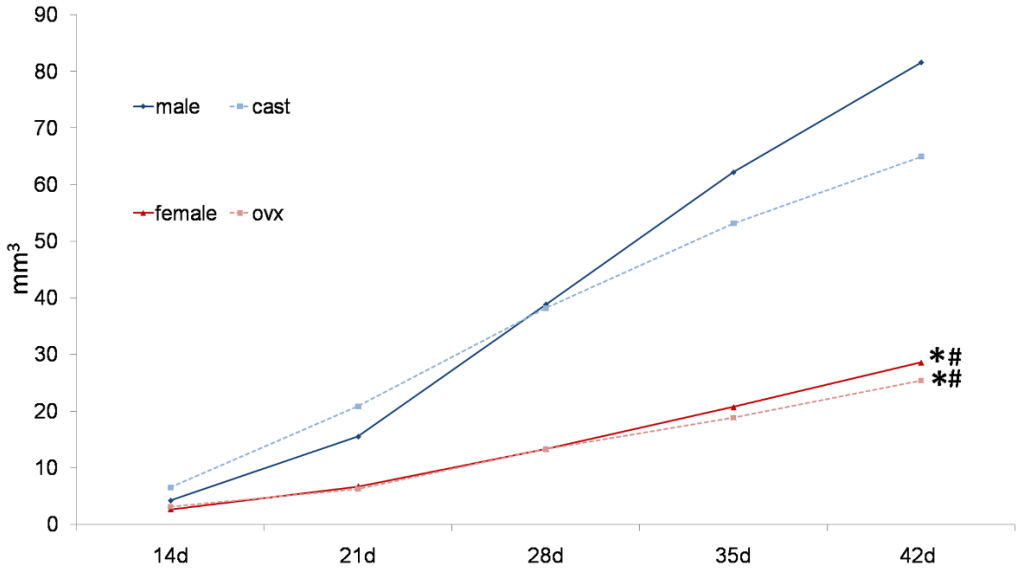

Figure 3. Rate (mm^3/day) of ectopic bone formation

Slope of the lines represent the rate of ectopic bone formation in male, castrated, female and ovariectomized hosts. * indicates significantly different (p>.05) from male hosts; # indicates significantly different (p>.05) from cast hosts. No significant differences were found between male and cast hosts or between female and ovx hosts.

2.3.3 Analysis of Unaltered Skeletal Muscle

To determine if differences seen in ectopic bone formation were the result of innate differences in the skeletal muscle, non-implanted and age matched hind limb muscles from all host groups (male, cast, female, and ovx) were analyzed for both muscle fiber type distribution and vascularity.

Significant differences in skeletal muscle fiber type composition were found between the following groups: male and castrated, female and ovariectomized, castrated and ovariectomized and male and female, as seen in Figure 4. However, these fiber type differences did not correlate with previously described ectopic bone volume or formation rate differences. Vascularity of hind

limb skeletal muscle was also examined via CD31 immunostaining, and no differences were found between any host groups (Figure 5).

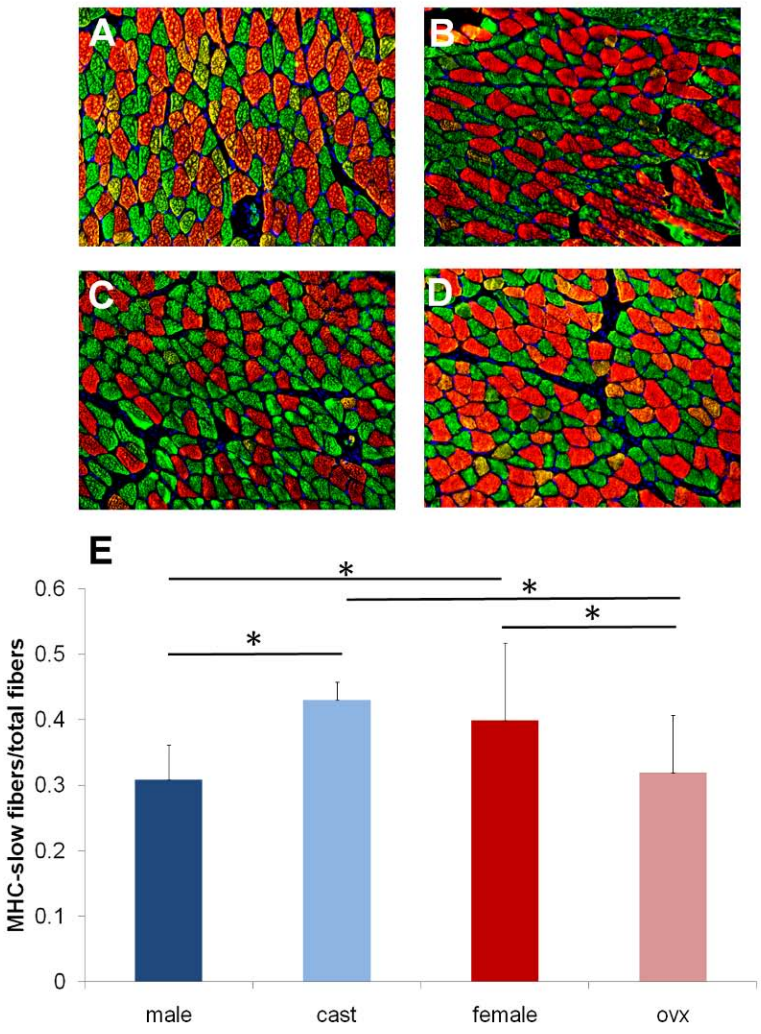

Figure 4. Fiber type analysis of non-implanted muscle.

Fiber type analysis of non-implanted hind limb muscle in all host groups (male, cast, female and ovx). In representative images A-D, MHC-slow isoform (slow twitch) fibers are stained red, MHC-fast isoform (fast twitch) fibers are stained green, and nuclei (DAPI) are stained blue. A) male host B) cast host C) female host D) ovx host E) quantification of MHC-slow fibers per total number of fibers. * indicates $p<.05$ and significant differences between male and cast hosts, male and female hosts, ovx and cast hosts, and ovx and female hosts.

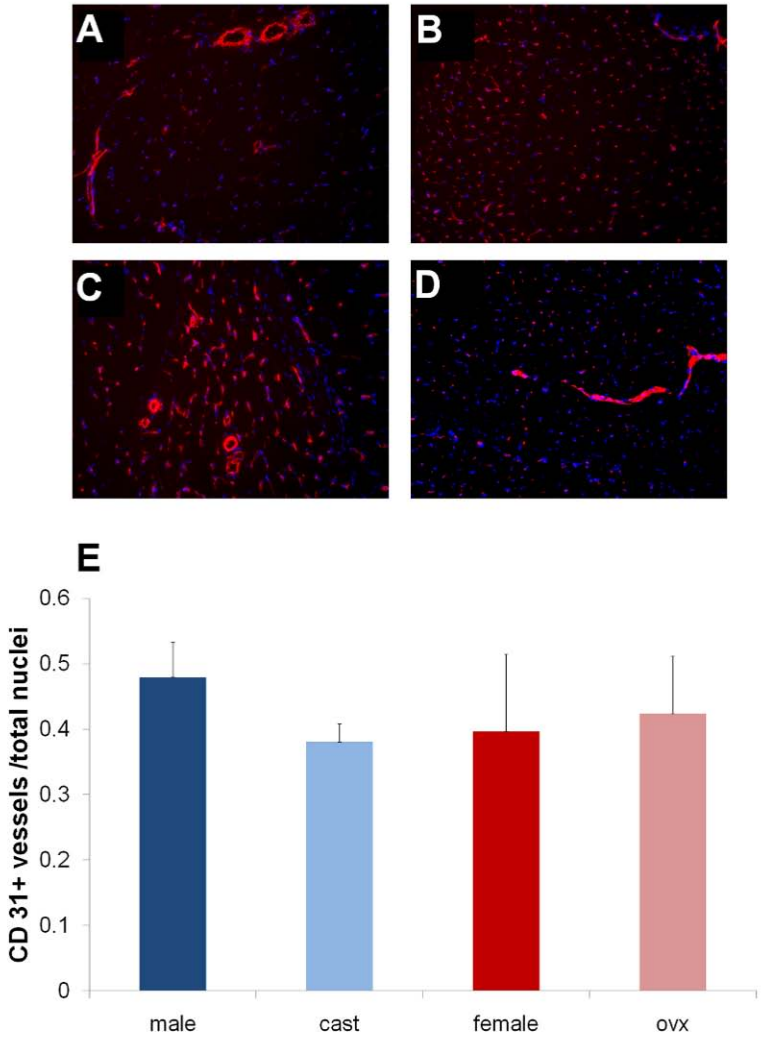

Figure 5. CD 31 analysis of non-implanted muscle.

CD 31 analysis of non-implanted hind limb muscle in all host groups (male, cast, female and ovx). In A-D, CD31 positive areas (blood vessels) are stained red and nuclei (DAPI) are stained blue. A) male host B) cast host C) female host D) ovx host E) quantification of CD31+ vessels per total nuclei. No significant differences in vascularity were found among any host groups.

2.3.4 Histological Analysis

Because no differences in volume or rate of ectopic bone formation were seen between hosts of the same sex, i.e. male and castrated hosts and female and ovariectomized hosts, only male and female host groups were histologically analyzed. At 21 and 42 days post implantation of MDSC-B4 infused gelatin sponges, samples from both male and female hosts were examined using H&E and Alcian Blue stains, as well as GFP immunostaining. Through these histological analyses, the process of endochondral ossification which results in ectopic bone formation can be evaluated. Additionally, the contribution of both donor and host-derived cells can be determined.

2.3.4.1 H&E Staining

Representative images of MDSC-mediated ectopic bone formation in both male and female hosts at 21 and 42 days post implantation are shown in Figure 6. Male hosts display bone tissue at both 21 and 42 days, with the latter time point exclusively showing mature lamellar bone with fat and blood cell filled spaces, resembling marrow cavities. In contrast, female hosts at 21 days display large clusters of chondrocytes with no apparent bone tissue. By 42 days, a shell of bone tissue is surrounding the chondrocytes clusters, but it appears to be less mature bone, and no marrow-like spaces are seen.

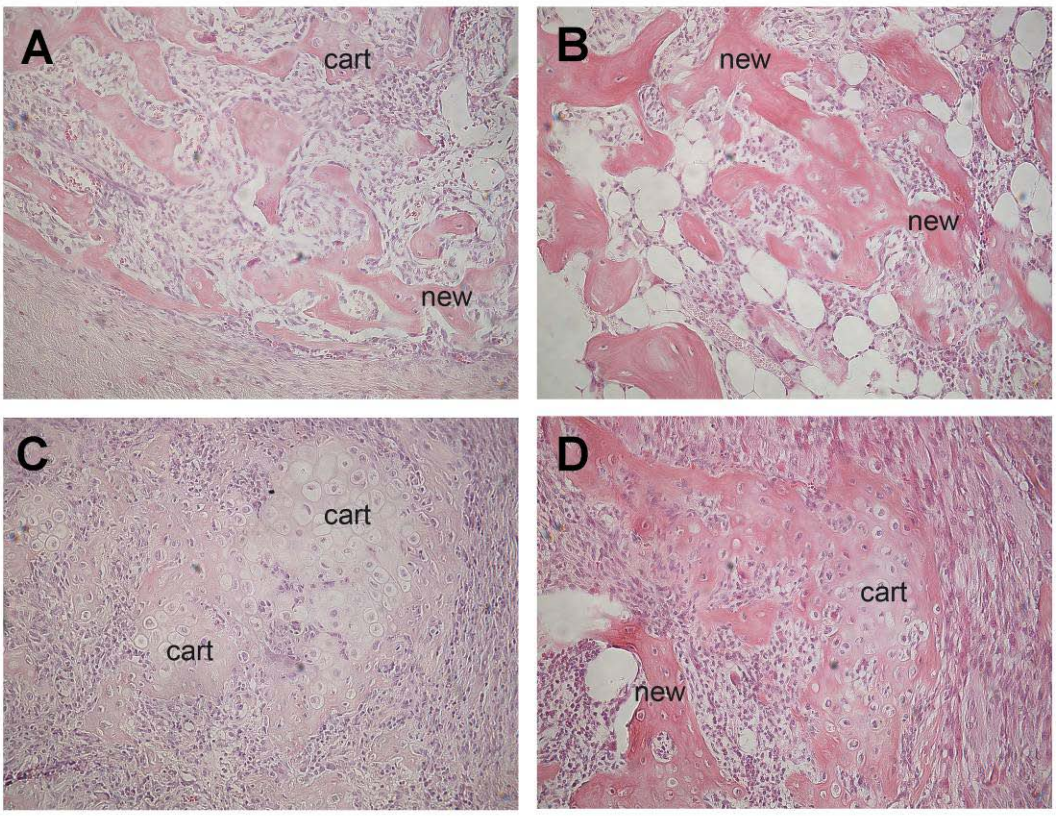

Figure 6. H&E staining of ectopic bone

Hematoxylin and eosin staining of intramuscular ectopic bone showing general morphology and tissue type: cart – cartilage, new – new bone. A) male host at 3 weeks post implantation B) male host at 6 weeks post implantation C) female host at 3 weeks post implantation D) female host at 6 weeks post implantation.

2.3.4.2 Alcian Blue Staining

Alcian blue, which stains the glycosaminoglycans present in cartilage extracellular matrix, was also utilized, along with a counterstain of nuclear fast red to more precisely examine the cartilage phase of endochondral ossification leading to MDSC-mediated ectopic bone formation in male and female hosts. Similar to findings of H&E staining, Alcian blue staining in Figure 7 showed little cartilage present in male hosts at 21 days post implantation and no glycosaminoglycan

containing cartilage matrix at 42 days post implantation, indicating mature ectopic bone. Conversely, abundant glycosaminoglycan cartilage matrix is present at both 21 and 42 days post implantation in female hosts, indicating ectopic bone in earlier stages of endochondral ossification.

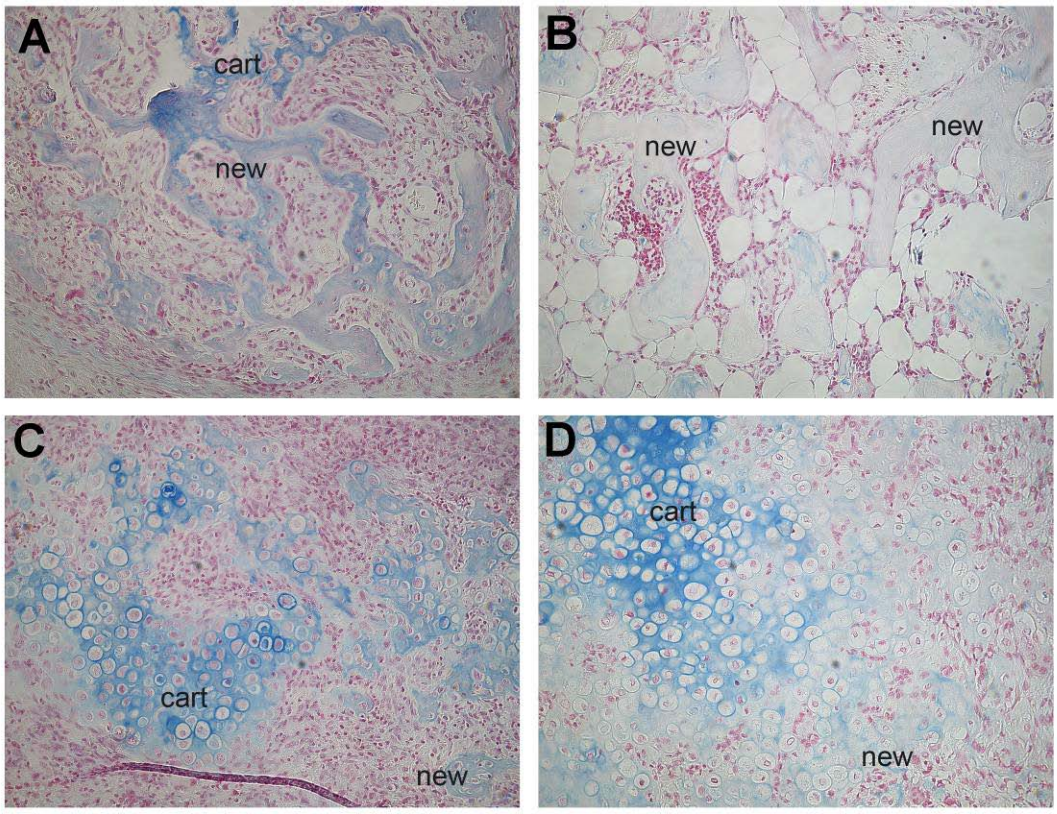

Figure 7. Alcian Blue staining of ectopic bone

Alcian Blue staining of intramuscular ectopic bone showing cartilage matrix (blue) and nuclei (red); new – new bone, cart - cartilage. A) male host at 3 weeks post implantation B) male host at 6 weeks post implantation C) female host at 3 weeks post implantation D) female host at 6 weeks post implantation.

2.3.4.3 Identification of Host and Donor Cells

To determine the contribution of donor and host cells to ectopic bone formation, immunostaining for GFP was performed. As seen in Figure 8, in both male and female hosts, donor cells were found, but host derived cells predominate in the ectopic bone tissue. Moreover, in both host groups, donor cells participated in all aspects of endochondral bone formation. Donor cells are observed as chondrocytes, osteoblasts, and osteocytes. However, only cells from the host fill the marrow-like spaces.

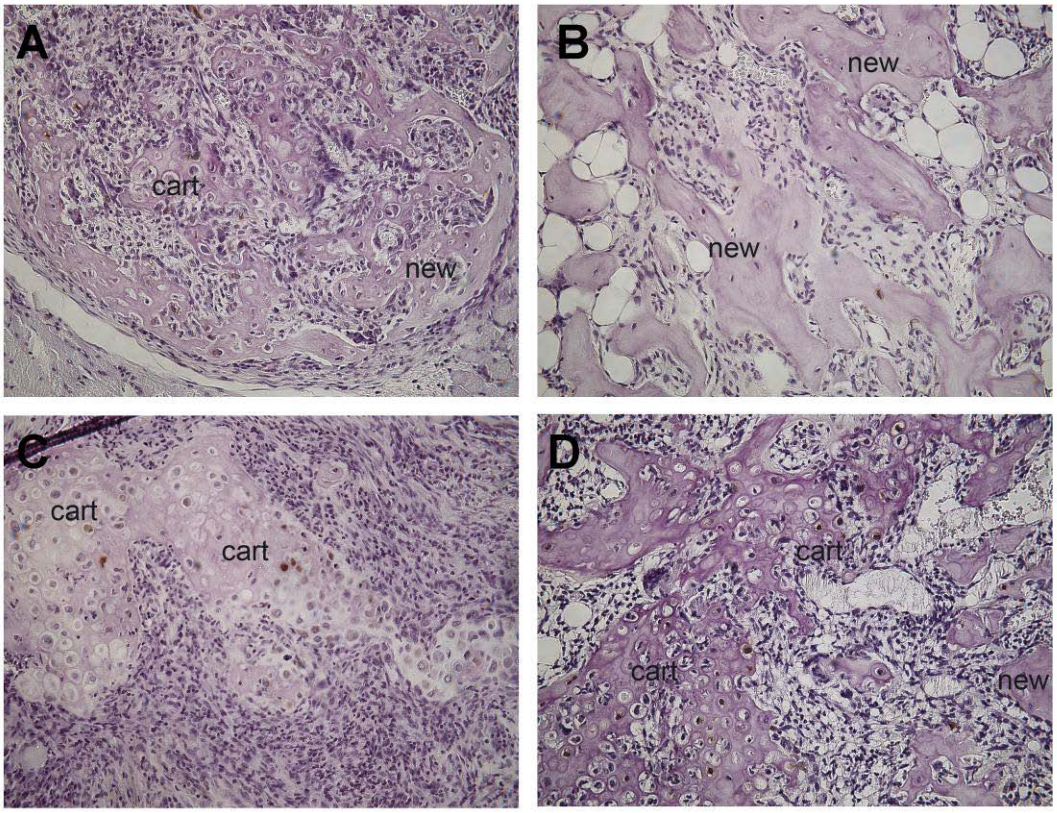

Figure 8. GFP staining of ectopic bone

GFP staining staining of intramuscular ectopic bone showing donor-derived cells (brown) and host-derived cells (purple); cart – cartilage, new – new bone. A) male host at 3 weeks post implantation B) male host at 6 weeks post implantation C) female host at 3 weeks post implantation D) female host at 6 weeks post implantation.

2.4 DISCUSSION

Previous MDSC differentiation studies, which found significant differences in osteogenic, chondrogenic and myogenic differentiation (both in vivo and in vitro) based on donor sex in addition to in vivo differences in muscle repair correlated to host animal sex [18-20]. This study examined the effect of host sex and sex hormones on MDSC-mediated in vivo ectopic bone formation. Using four host animal groups (unaltered male, castrated male, unaltered female, and ovariectomized female) and an ectopic intramuscular bone formation model, analyses of bone volume, rate of formation, and histological stains were performed.

Using microCT analysis, volume of ectopic bone formed was calculated at 14, 21, 28, 35 and 42 days post implantation of MDSC-B4 filled gelatin sponge in the hind limbs of all host animal groups. At all time points except 14 days, male hosts (whether unaltered males or castrated males) displayed significantly more bone formed than female hosts (whether unaltered females or ovariectomized females). These data suggest that sex hormones do not affect MDSC-mediated ectopic bone formation because no volume differences were seen between male and castrated groups or between female and ovariectomized groups. These results are in contrast to previous ectopic bone formation studies, utilizing demineralized bone matrix (DBM), which show sex hormone effects in multiple species. Burnett and Reddi found that estrogen and progesterone (hormones that would decrease with ovariectomy) are stimulatory in DBM-induced ectopic bone formation in rats [80]. Kapur and Reddi also determined that DBM-induced ectopic bone formation is decreased in castrated rats, and androgen administration stimulates ectopic bone formation in these animals [81]. In mice, DBM-induced ectopic bone formation is known to be decreased in ovariectomized hosts, and estrogen replacement can reverse this decrease [82]. In regards to native bone maintenance and turnover, ovariectomy is also known to decrease bone

volume and quality in both rats and mice (including the C57BL strain of mice used in this study) [83-87]. On the other hand, one study shows increased bone accretion in female C57BL mice following ovariectomy [88]. Normal skeletal bone formation, growth and maintenance are all known to be influenced by sex steroid hormones [89-91]. However, MDSC-mediated bone formation appears to not be influenced by ovariectomy or castration, which could be promising for translation to clinical therapies. As ovariectomy and castration are sometimes used as models of aging, and perhaps bone tissue engineering therapies utilizing MDSCs could prove to be more effective in aged patients than matrix-based counterparts.

Because ectopic bone volume measurements varied significantly between sexes (but not between hosts of the same sex), the question was raised – are female hosts (both unaltered and ovariectomized) just exhibiting delayed bone formation and given enough time, will they eventually 'catch up' to the males hosts? All experiments were concluded at 42 days post implantation due to the large volume of bone formed in the male and castrated hosts, so an empirical answer cannot be concluded. However, upon examination of μCT volume data in terms of rate of bone formation, the extrapolated conclusion would be that female hosts will never 'catch up' to male hosts in MDSC-mediated ectopic bone formation assays. Via two-way repeated measures ANOVA, it was determined that the rate of bone formation (the slope of the lines in Figure 3) is statistically different between male hosts and both female and ovariectomized hosts, as well as between castrated hosts and both female and ovariectomized hosts. If female hosts were ever to 'catch up' with male hosts, it would require that the slope of the female rates would be steeper than that of the males hosts, in order for the rate lines to intersect. These data also indicate that it is not merely a delay in female host bone formation that causes significant differences in volumes at various time points because if that were true, male

and female hosts would display similar rate curves, with female and ovariectomized hosts shifted to the right (later in time). However, what can be reasoned from these data is male and castrated hosts form MDSC-mediated ectopic bone at a completely different rate than female and ovariectomized hosts, possibly indicating a different manner of bone formation.

After determining that male hosts (both unaltered and castrated) form more MDSC-mediated intramuscular ectopic bone at a faster rate than their female counterparts (both unaltered and ovariectomized), it was hypothesized that innate differences in the skeletal muscle environment could account for the different mode of bone formation. Stem cells, and more specifically, human osteoprogenitor cells, are believed to be associated with and located near blood vessels [92-94]. Greater number of skeletal muscle blood vessels could indicate more osteoprogenitors and provide a rationale for differences seen between hosts of different sexes. Moreover, Tie2-expressing endothelial precursors associated with blood vessels have been implicated as osteoprogenitors directly contributing to ectopic endochondral ossification in a mouse model of fibrodysplasia ossificans [95]. Skeletal muscle fiber type is also known to correlate with vascularity. Due to metabolic demands, slow twitch muscle fibers require more oxygen and consequently have more blood vessels than fast twitch muscle fibers [34]. Therefore, both skeletal muscle fiber type and vascularity were assessed in all host groups, via myosin heavy chain isoform and CD 31 immunostaining respectively. Many significant differences were found in fiber type distribution among the four host groups. Correlating with bone volume findings, castrated host muscle contains more slow twitch fibers than ovariectomized host muscle; however, inconsistent with bone volume findings, female host muscle contains more slow twitch fibers than male host muscle. Additional fiber distribution significant differences between both castrated and male hosts and between ovariectomized and female hosts were

found, groups where no differences were found in ectopic bone volume; these results are in contrast to studies in rats showing no changes in fiber type distribution following ovariectomy or castration [96, 97]. Surprisingly no significant differences were found between any host groups in the CD 31 positivity of skeletal muscle, which does not correlate with fiber type distribution findings. Most importantly, no correlation was found between vascularity of skeletal muscle tissue and the volume of MDSC-mediated ectopic bone in unaltered male, castrated male, unaltered female and ovariectomized hosts. This could be a consequence of the way that vascularity was measured and quantified in this study (via CD31 immunostaining) or that CD31 immunostaining does not identify the same blood vessel associated cells as Tie2 immunostaining. It was also not determined if the CD31 positive cells found in native skeletal muscle directly differentiate into the bone tissue induced by MDSC-B4. However, based on the available evidence, vascularity, and by extension blood vessel-associated osteoprogenitor cells, were not determined to be the cause of differences in MDSC-mediated ectopic bone formation.

A factor that could play a role is non hormone related sex differences in gene expression of the skeletal muscle environment surrounding and contributing to the MDSC-mediated ectopic bone formation. Of the 7367 genes expressed in murine skeletal muscle, 55.4% of these are sexually dimorphic [98]. Interestingly, 4 of these sexually dimorphic skeletal muscle genes are also known to be involved in BMP induced endochondral ossification [99].

While volume and rate of MDSC- mediated ectopic bone formation are different between hosts of different sexes, i.e. male and female hosts, male and ovariectomized hosts, castrated and female hosts, castrated and ovariectomized hosts, no differences were found between hosts of the same sex (male and castrated hosts or female and ovariectomized hosts). Additionally, from histological analyses of muscle without MDSC-B4 gelatin sponges, no conclusions could be

made about correlations of fiber type or vascularity and volume of ectopic bone. Therefore, it is assumed that male and castrated male hosts and female and ovariectomized female hosts are similar, and only male and female hosts, not castrated males or ovariectomized hosts, were used for histological analyses of endochondral ectopic bone formation.

Both H&E and Alcian blue staining of MDSC-mediated ectopic bone formation at 21 and 42 days post implantation support the same conclusion – implants in male hosts undergo endochondral ossification faster than female hosts. At both 21 and 42 days post implantation, male hosts show predominantly bone matrix, with only small islands of glycosaminoglycan positive cartilage matrix, while female hosts, at both time points, display large hypertrophic chondrocytes surrounded by abundant cartilage matrix, with a thin shell of bone matrix surrounding. These data suggest again that female hosts are not merely delayed in their bone formation compared to male hosts, but instead, male and female hosts form MDSC-mediated ectopic bone in different manners. If female hosts were delayed, histological analyses of females at 42 days would be similar to male hosts at 21 days post implantation, as these time points are when similar ectopic bone volumes are seen (Figure 2). However, it seems that endochondral ossification in male hosts is hastened; males turnover cartilage into bone much more rapidly than female hosts. The rate of endochondral bone formation and turnover from cartilage to bone is the reason for disparate volumes seen in male (unaltered or castrated) versus female (unaltered or ovariectomized) hosts, as time-volume interactions between groups demonstrated (Figure 3) and histological analyses (Figure 6 &Figure 7) further support.

While it was demonstrated that male and female, as well as castrated and ovariectomized hosts, all undergo endochondral ossification of tissue surrounding MDSC-B4 gelatin implants, differences in the volume of bone formed and the rate of the bone accretion between hosts of

different sexes were seen. This was attributed to faster endochondral bone formation, via more rapid turnover of tissue from cartilage to bone, in male hosts compared to female hosts. However, the reason for this more rapid turnover was unknown. Therefore, it was investigated if the survival of donor MDSC-B4, which are the inducers of the endochondral bone formation, is different in male and female hosts. Since MDSC-B4 cells were also tagged with GFP, immunostaining for GFP was used to track these cells at 21 and 42 days post implantation in male and female hosts. Throughout the stages of endochondral ossification, which are accelerated in male hosts, MDSC-B4 donor cells are found, and they appear in all phases of endochondral ossification (Figure 8). MDSC-B4 cells are present as chondrocytes, osteocytes, and osteoblasts. However, MDSC-B4 cells are not seen in the marrow-like spaces of the more mature male host bone at 42 days; only host cells are seen there. There is no marked difference between the number of MDSC-B4 cells present in male and female hosts at either 21 or 42 days post implantation. Therefore, it is concluded that although male and female hosts form differing amounts of bone in response to MDSC-B4 implantation and this is due to a faster rate of endochondral bone formation in male hosts, survival of donor cells is not a contributing factor to this rate difference.

2.5 CONCLUSIONS

This study aimed to evaluate the role of host animal sex and sex hormones in bone formation by examining an MDSC-mediated endochondral bone formation model in male, castrated male, female, and ovariectomized female mice. Two hypotheses were tested: more MDSC-mediated

intramuscular ectopic bone formation will occur in male than in female host animals, and castration and ovariectomy will not affect MDSC-mediated bone formation sex differences. Indeed, more ectopic bone formed in male hosts than in female hosts, and this ectopic bone also formed at a faster rate. However, castration and ovariectomy did not negatively affect bone formation; unaltered male and castrated hosts displayed similar bone volume and formation rates, as did unaltered female and ovariectomized hosts. CD 31 positivity and fiber type distribution of the skeletal muscle environment were determined to not correlate with ectopic bone volume or formation rate. Ectopic bone formation was also not correlated to survival of donor cells in the skeletal muscle. The paramount factor for ectopic bone formation differences in this model appears to be the rate of turnover from cartilage to bone during the endochondral bone formation process, and this is supported by both bone formation rate quantitative data and histological analyses. Male hosts, whether unaltered or castrated, form more ectopic bone at a faster rate than female hosts, whether unaltered or ovariectomized, because during endochondral bone formation male hosts remodel cartilage into bone at a faster rate than female hosts.

3.0 EFFECT OF HOST SEX ON BONE HEALING MEDIATED BY MDSCS

3.1 INTRODUCTION

After it was determined that MDSC-mediated ectopic bone formation occurs faster in male and castrated hosts compared to female and ovariectomized hosts, the effect of host sex and sex hormones on bone healing was examined. MDSC-induced healing in a mouse critical-size cranial defect model was studied in unaltered male, castrated male, unaltered female, and ovariectomized female hosts using microCT and histological analyses. The hypotheses of this study were as follows: one, MDSC-mediated cranial defect healing will be superior in male compared to female host animals, and two, castration and ovariectomy will not affect MDSC-mediated bone healing sex differences.

3.2 METHODS

3.2.1 MDSC Isolation and Retroviral Transduction

Cells were isolated, cultured, retrovirally transduced and stored in the same manner as described in section 2.2.1.

3.2.2 Surgical Procedure

For cranial defect healing assays, four host animal groups were used: unaltered male, unaltered female, castrated male, and ovariectomized female C57BL/10J mice. All animals were purchased from Jackson Laboratories, and castration and ovariectomy were performed prior to acquisition at age 5 weeks. Surgeries were performed at age 12 weeks. After sacrifice, castration or ovariectomy were visually confirmed.

Following sterile surgical procedures outlined in the University of Pittsburgh IACUC Protocol #0807916, each animal was anesthetized and an incision was made along the frontal and parietal bones of the skull. To create the cranial defect, the scalp was dissected and 5 mm trephine was used to create the circular bone defect. Just prior to treatment, 500,000 MDSC-B4 were mixed with sealer protein solution, and this mixture was applied to the defect simultaneously with thrombin solution. The sealer and thrombin solutions are components of Tisseel fibrin sealant kit (Baxter Biosurgery), and total volume was ~40uL of fibrin sealant. The incisions were then closed with sutures and the animals were allowed to resume normal activity. Animals were sacrificed at various time points following treatment: 2, 4, 7, 10, 14 and 28 days.

3.2.3 microCT Analysis

Healing of the cranial defect was evaluated in all groups with a μCT scanner (VivaCT40, Scanco Medical) at 14 and 28 days post treatment. Mice were anesthetized and positioned in an animal scanning bed with the skull in specially designed holder. Scanning was performed with the following settings: energy of 55 kVp, intensity of 145 μA, nominal resolution of 35 μm, and

integration time of 200 ms. Two-dimensional image slices were obtained and contour lines were drawn to define volume of interest (VOI). An appropriate threshold was chosen for the bone voxels by visually matching thresholded areas to grayscale images. The threshold was kept constant throughout the analyses. This led to a three-dimensional reconstruction of the ectopic bone and provided quantitative data on bone volume (mm^3).

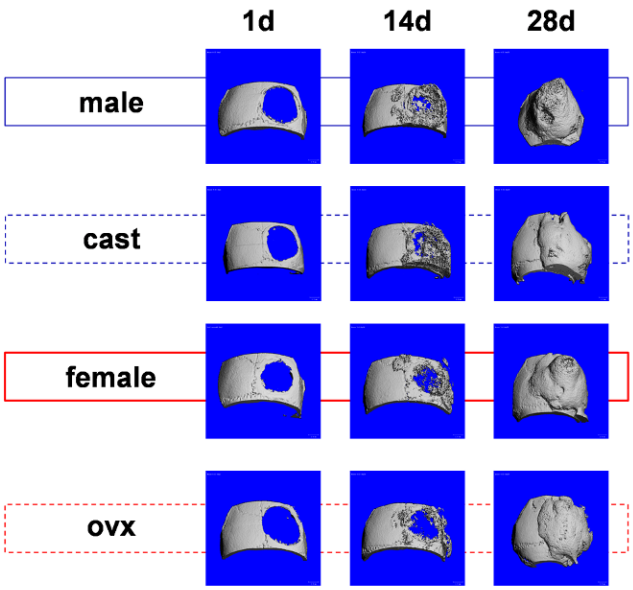

Figure 9: Representative microCT reconstructions of cranial defects

In order to compare with previous studies which quantified non-healed area of defect from planar radiographs, three-dimensional reconstructions were analyzed using Northern Eclipse imaging software. First, a calibration of pixel number to distance on the scale bar of the three-dimensional reconstruction was performed. Then, the image was changed to grayscale and thresholds were applied to determine the area of the black region selected (inside the yellow boundary). Planar area of defect was computed for every animal in each host group (8-11

animals) at 14 days post treatment, and resulting data are displayed as mean ± standard deviation. Planar area was not computed at 28 days post treatment because all animals in all groups showed complete defect coverage at this time point.

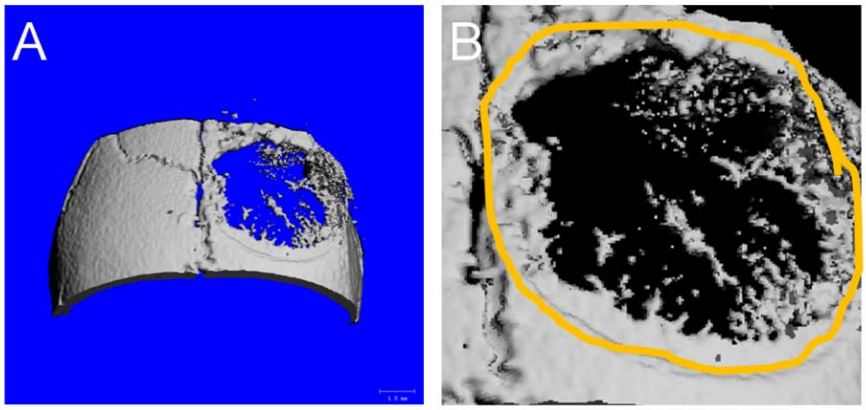

Figure 10: Quantification of planar area of cranial defect

A) Representative microCT reconstruction of defect at 14 days post implantation B) Determination of area of defect using Northern Eclipse software

In addition to defect area measurements, volume measurements were computed for both total new bone formed, as well as bone formed within the defect, for each animal at 14 and 28 days post treatment. For each two-dimensional slice, areas encompassing all bone formed (including rounding and healing of defect margins) were drawn. Volume of total new bone was the computed for each sample (8-11 animals per group, at both 14 and 28 days post treatment). Later, total new bone volume areas drawn on each slice were edited and modified to only include new bone formed within the defect (including rounding and healing of defect margins, but only to the thickness of native skull). From these areas, volume of within defect bone formed was computed for each sample sample (8-11 animals per group, at both 14 and 28 days post treatment). All volume data are displayed as mean ± standard deviation.

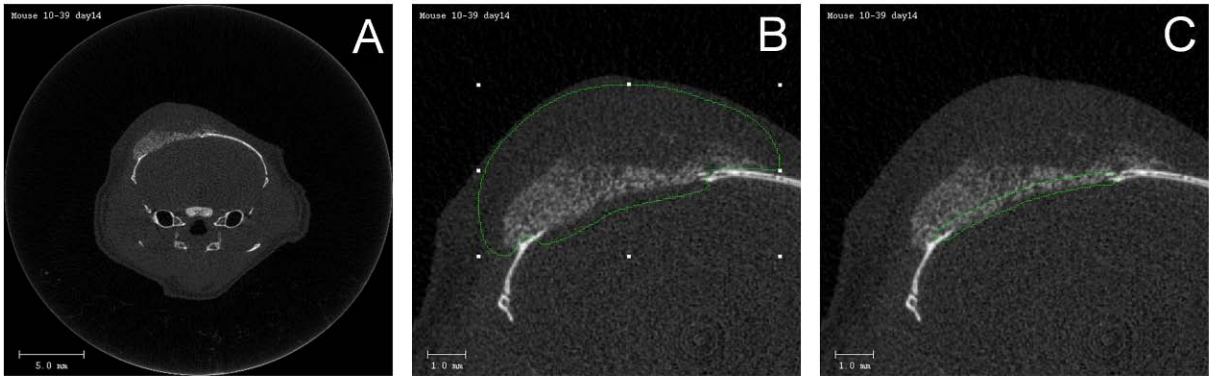

Figure 11: Quantification of total new bone volume and within defect bone volume

A)Representative slice of microCT scan B) determination of total bone volume C) determination of within defect bone volume

It is important to evaluate the location of bone formed, in addition to quantifying how much bone is formed. A numerical index termed “spatial control index” was also calculated, and it is defined as (within defect bone volume/ total bone volume) *100%. Therefore, a spatial control index of 100% would indicate that all bone formed during the healing process was formed only within the cranial defect; however, a value of 100% does not mean the defect is completely healed.

3.2.4 Histological Analyses

After euthanasia, the skulls, with the mandibles and skin removed, were placed in formalin (3.7% neutral buffered formaldehyde) for 24 hours. The samples were then decalcified in 10%

EDTA (Sigma-Aldrich). Dehydration and then paraffin embedding followed, and samples were cut with a microtome into 5 micron sections and dried.

Following deparaffinization and rehydration, sections of bone containing the defect area were stained using standard procedure for hematoxylin and eosin staining (H&E) to determine general tissue morphology. Donor cells were distinguished from host cells by staining for GFP, since all donor cells are producing both GFP and BMP4. Briefly, after blocking in both 3% H_2O_2 in methanol and 2% horse serum in PBS, biotintylated anti-GFP antibody (Vector Laboratories) was applied at a 1:1000 dilution. Then, streptavidin/HRP (R&D) was applied at a 1:50 dilution followed by DAB Peroxidase Substrate Kit (Vector Laboratories) per manufacturer's instructions. Hematoxylin QS (Vector Laboratories) was used as a counterstain. Resultant stain shows donor cells expressing GFP (MDSC-B4) as brown and all cells from the host as purple.

All images were taken on Nikon Eclipse E800 microscope equipped with a Retiga EXi digital camera using QCapture for brightfield images.

3.2.5 Statistical Analysis

All numerical values (planar area, within defect volume, total volume, spatial control index) were computed using microCT measurements from 8-11 animals per host sex group: male, castrated male, female and ovariectomized female. Statistical analyses (ANOVA or repeated measures ANOVA) were performed with SPSS, and differences were considered significant if $p<.05$.

3.3 RESULTS

A critical size cranial defect was created in male, castrated, female and ovariectomized hosts and then treated with MDSC-B4 in fibrin to induce bone formation and healing of the defect. Using microCT scanning and histological analysis, differences in healing between the four host groups was observed.

3.3.1 Planar Area of Defect

Following microCT scanning, a three-dimensional reconstruction of each defect area was created, and this reconstruction was then processed to determine area of defect remaining at 14 days post treatment. Scans were also taken at 28 days post treatment, but all groups displayed total coverage of the defect area (see Figure 9), so planar area was not computed at 28 days post treatment. Ovariectomized host displayed the largest defect area, corresponding to less healing, at 14 days post treatment with MDSC-B4 (see Figure 12).

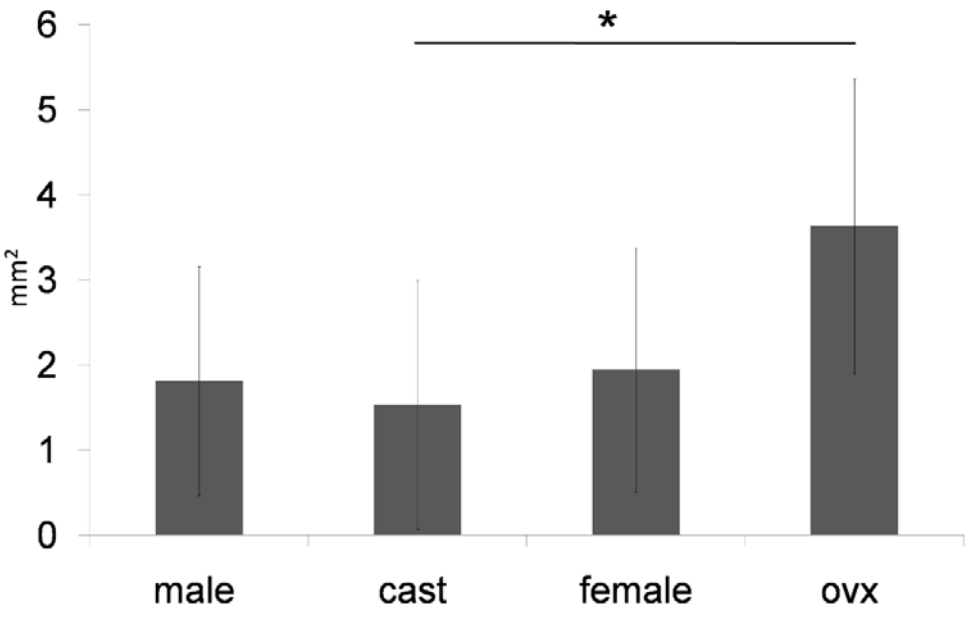

Figure 12: Planar area of defect

Area of defect (mm^2) after 14 days of treatment with MDSC-B4. * indicates p>.05

3.3.2 Bone Volume Formed after MDSC Treatment

Both within defect bone volume and total bone volume formed were quantified for each host sex group at both 14 and 28 days post treatment. Each host sex group displayed significantly more bone at 28 days post treatment than at 14 days, and female hosts (both unaltered female and ovariectomized female) showed significantly less within defect bone than castrated hosts at 28 days. Moreover, at 28 days post treatment total bone volume was significantly less in female hosts when compared to male hosts. Ovariectomized hosts also showed significantly less total bone volume than castrated hosts at 14days post treatment with MDSC-B4.

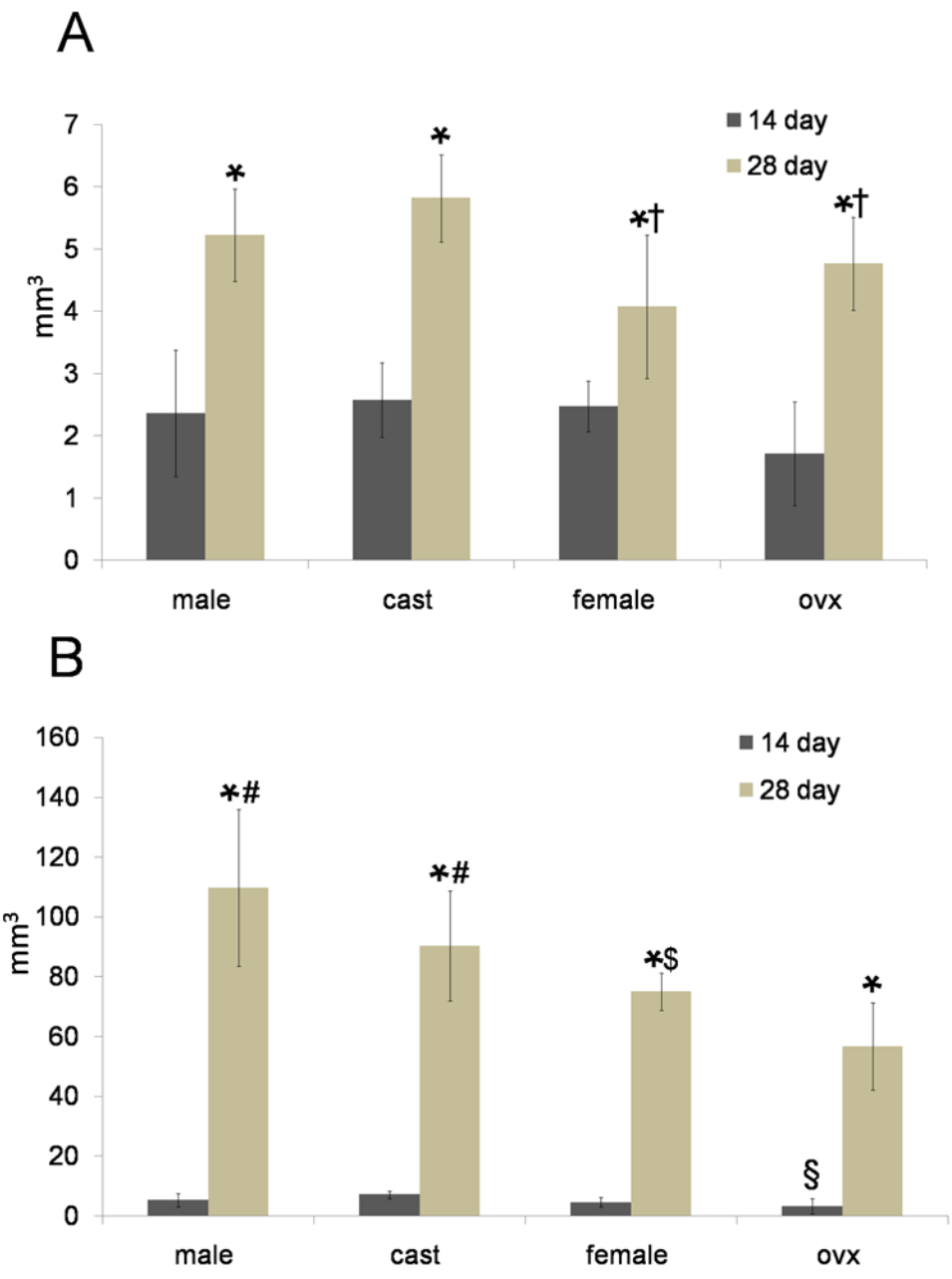

Figure 13: Within defect and total new bone volume

A) Within defect bone volume (mm^3) after 14 and 21 days of treatment with MDSC-B4 B) Total new bone volume (mm^3) after 14 and 21 days of treatment with MDSC-B4. All statistical notations indicate $p<.05$. * from same group at 14 days, § from cast at 14 days, # from ovx at 28 days, $ from male at 28 days, † from cast at 28 days.

3.3.3 Spatial Control Index of Defect Healing

From the three-dimensional reconstructions, as well as quantification of within defect bone volume and total bone volume, it was apparent that not all bone formed following application of MDSC-B4 was within the defect space – a great deal of bone formed on top of the skull. Therefore, the measure of spatial control index (within defect bone volume/ total bone volume * 100%) was computed for each host sex group at 14 and 28 days post treatment. All hosts sex groups significantly decreased spatial control index from 14 days to 28 days, but at 14 days post treatment, female and ovariectomized hosts have higher spatial control index than male and castrated hosts. While this measure at 28 days decreased in all groups, spatial control index in ovariectomized females was significantly larger than in unaltered female or male hosts.

Table 1: Spatial Control Index of Bone Formation in Host Sex Groups

	male	**cast**	**female**	**ovx**
14d	45.93%	37.70%	62.14% §	59.42% §
28d	4.88% *#	6.55% *	5.38% *#	8.49% *

All symbols indicate $p<.05$. * from same group at 14 days, § from cast at 14 days, # from ovx at 28 days

3.3.4 Histological Analyses

H&E staining and GFP immunostaining were performed on sections of each host sex group at various time points post treatment in order to evaluate MDSC-B4 mediated bone formation and healing of the critical size cranial defect. Unlike the previously described ectopic bone study, host groups of the same sex (unaltered/castrated male and unaltered/ovariectomized female) did have significant differences in some microCT measures; therefore all four host groups were examined. Representative images are shown for all groups at 2, 4, 7, 10, 14 and 28 days, except no images are available for unaltered male hosts at 14 days due animal deaths.

3.3.4.1 H&E Staining

In unaltered male hosts, representative images of H&E staining (Figure 14) demonstrate the healing and bone formation process. At 2 days post treatment, the defect margins and fibrin scaffold are present. At 4 days, larger numbers of unidentified mononuclear cells are present in an infiltration or proliferative phase, and the fibrin begins to degrade. Then, at 7 and 10 days post treatment, bone is present and starting to form into a trabecular network. At 28 days post treatment, an arrangement of mature trabecular bone is observed with marrow-like spaces filled with red blood cells. Even though extensive bone eventually forms over the critical size cranial defect, it is not similar to the compact, flat bone normally observed in the skull.

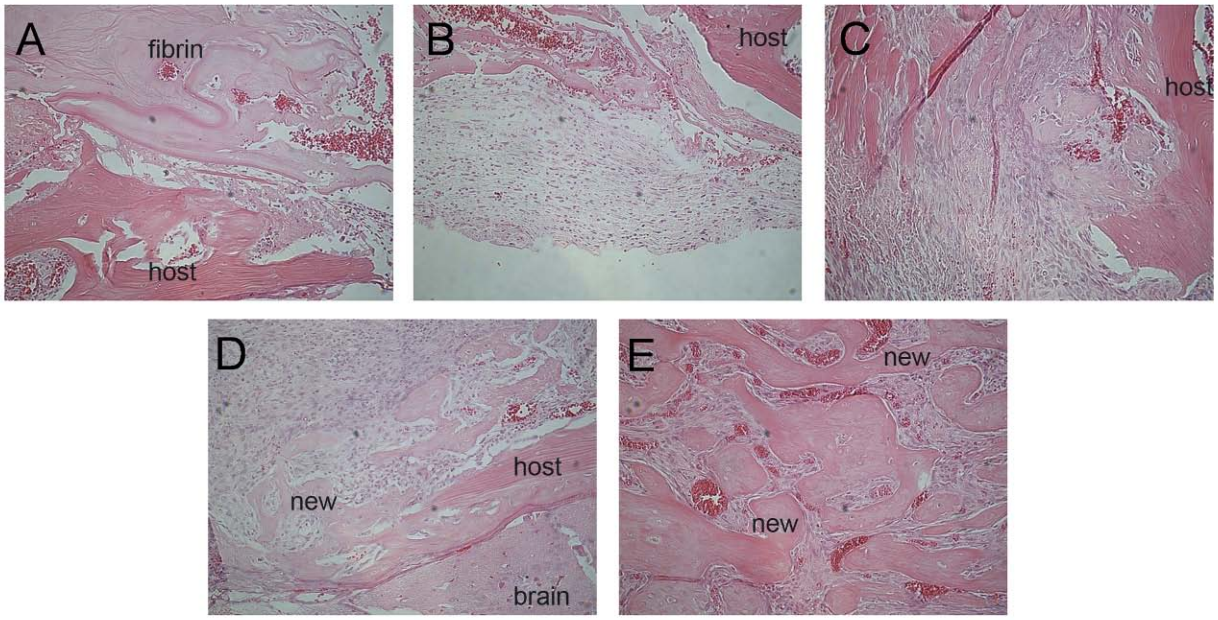

Figure 14: H&E staining of cranial defect healing in male hosts

Representative images of H&E staining of cranial defect in male hosts at A) 2 days B) 4 days C) 7 days D) 10 days and E) 28 days post treatment with MDSC-B4. All images 200x. fibrin- fibrin scaffold, host- host bone, new- new bone tissue, brain- host brain

In castrated hosts (Figure 15), similar to unaltered male hosts, early time points (2 and 4 days) show fibrin with cells infiltrating or proliferating in the defect area. At 7 and 10 days post treatment, numerous cells are present in the defect area. At 14 days post treatment, the cartilaginous phase of endochondral bone formation prevails, and at 28 days post treatment, trabecular networks of bone with marrow-like spaces cover the defect area.

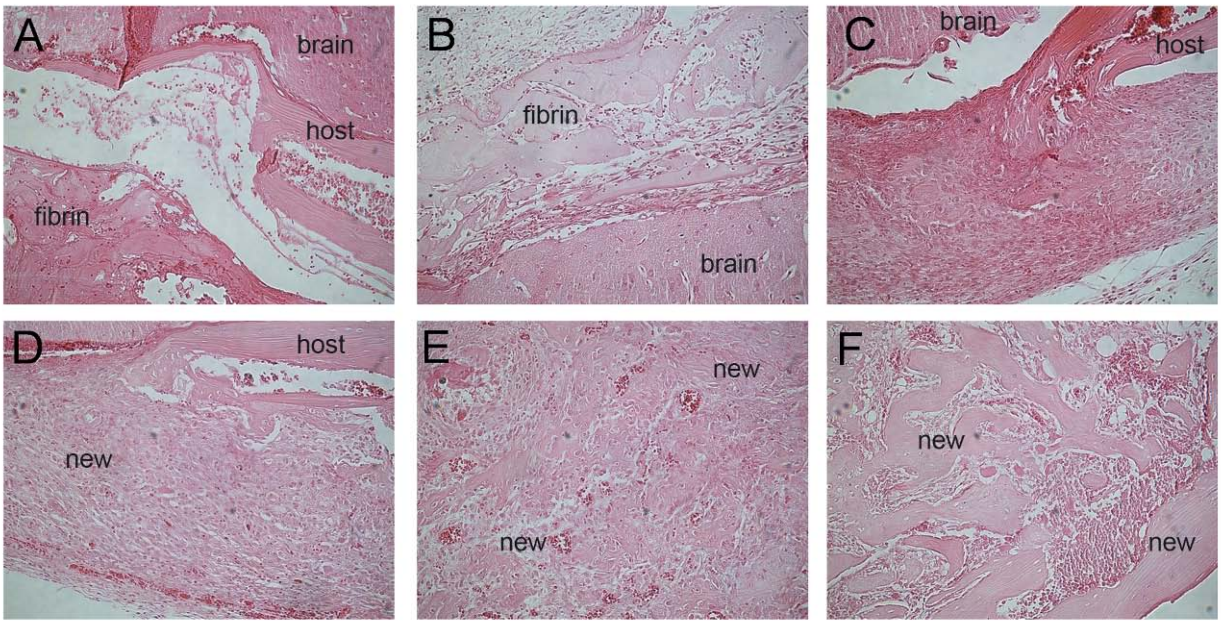

Figure 15: H&E staining of cranial defect healing in castrated hosts

Representative images of H&E staining of cranial defect in castrated hosts at A) 2 days B) 4 days C) 7 days D) 10 days E) 14 days and F) 28 days post treatment with MDSC-B4. All images 200x. fibrin- fibrin scaffold, host- host bone, new- new bone tissue, brain- host brain

In unaltered female hosts, representative H&E images tell a different story. At early time points (2, 4, 7 days post treatment), female hosts are similar to male (both unaltered and castrated hosts) in fibrin degradation and proliferative or infiltration response. However, at 10 days, this fibroproliferative phase persists. At 14 days post treatment, cartilage predominates new tissue and little bone is present. At 28 days, cartilage still remains, although some mature bone with marrow-like spaces is also present.

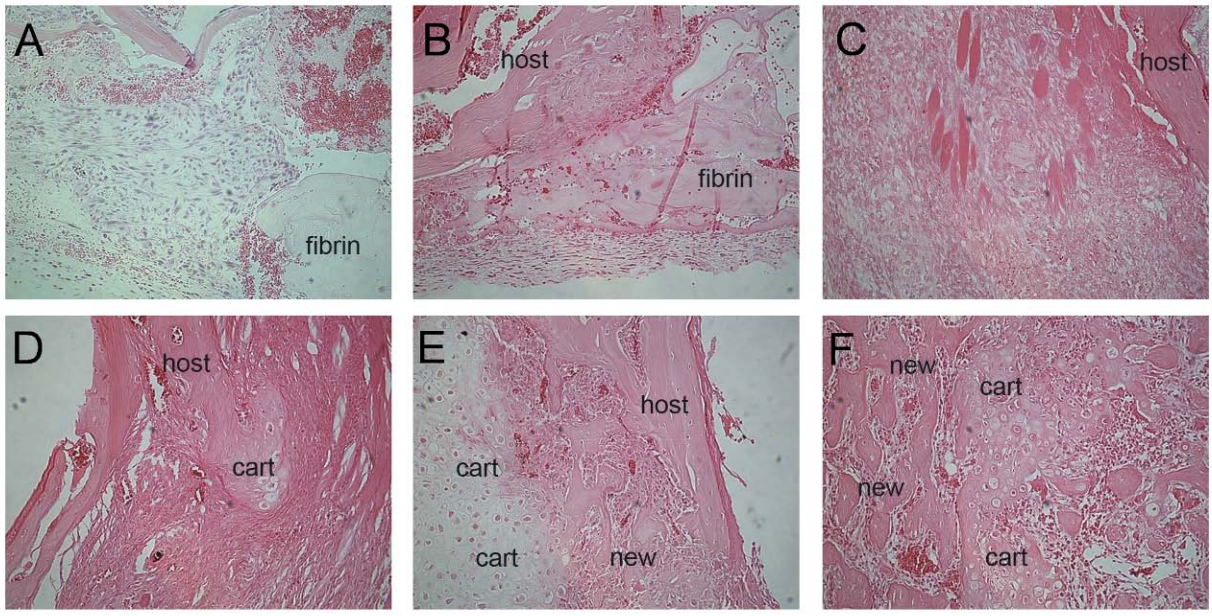

Figure 16: H&E staining of cranial defect healing in female hosts

Representative images of H&E staining of cranial defect in female hosts at A) 2 days B) 4 days C) 7 days D) 10 days E) 14 days and F) 28 days post treatment with MDSC-B4. All images 200x. fibrin- fibrin scaffold, host- host bone, new- new bone tissue, cart- cartilage

Ovariectomized female hosts are similar to unaltered female hosts in that they show a much slower progression of bone formation than unaltered or castrated male hosts. Like unaltered female hosts and both male host groups, ovariectomized female hosts show fibrin degradation and proliferative or infiltration response at early time points of 2, 4 and 7 days post treatment. Like unaltered female hosts, a continued fibroproliferative phase is present at 10 days post treatment. At 14 days post treatment, cartilage tissue with little immature bone is seen. At 28 days post treatment, cartilage tissue persists, with some mature bone with marrow-like spaces also observed.

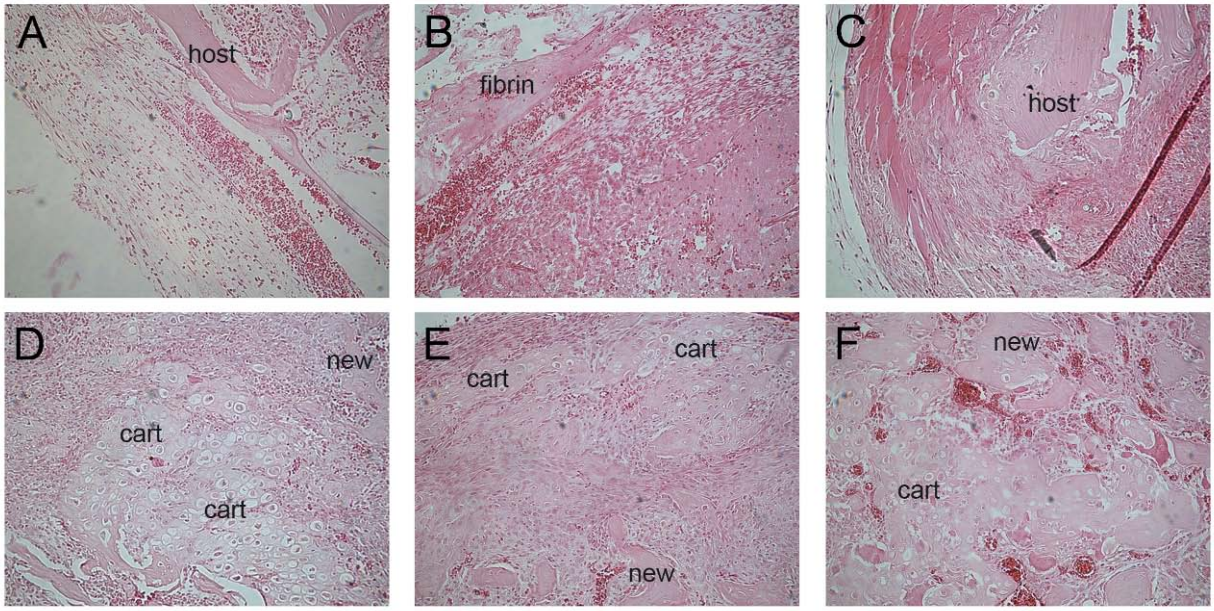

Figure 17: H&E staining of cranial defect healing in ovariectomized hosts

Representative images of H&E staining of cranial defect in ovariectomized hosts at A) 2 days B) 4 days C) 7 days D) 10 days E) 14 days and F) 28 days post treatment with MDSC-B4. All images 200x. fibrin- fibrin scaffold, host- host bone, new- new bone tissue, cart- cartilage

3.3.4.2 Identification of Host and Donor Cells

Using a peroxidase-based staining kit and an anti-GFP antibody, donor cells (stained brown in images) were distinguished from host cells (stained purple in images). In all host groups, donor cells were found at all time points, including 28 days post treatment, indicating that donor cells survive in the host animal. Moreover, donor cells were found participating in all aspects of endochondral bone formation; they are seen as small, mononucleated cells in the proliferative phase, and also as chondrocytes, osteocytes, and osteoblasts. Donor cells were never observed in the marrow-like spaces present in later stages of mature bone; these cells were always derived

from the host animal. Most importantly, the majority of cells participating in all stages of bone formation and healing of the defect were host derived, regardless of the sex group of the host.

In unaltered male hosts, the fate of donor-derived cells can be tracked throughout the formation of bone at the cranial defect site. However, at early time points, such as 2, 4 and 7 days post treatment, the donor cells remain small and rounded while interspersed with the infiltrating host cells at site of the defect and fibrin degradation. At 10 days post treatment, donor cells are still observed as small round cells, but at this time point, another phenotype of larger, flat donor cells are also seen. In the final stages of bone formation and healing of the defect, donor cells are seen as both osteocytes and osteoblasts in the mature bone tissue.

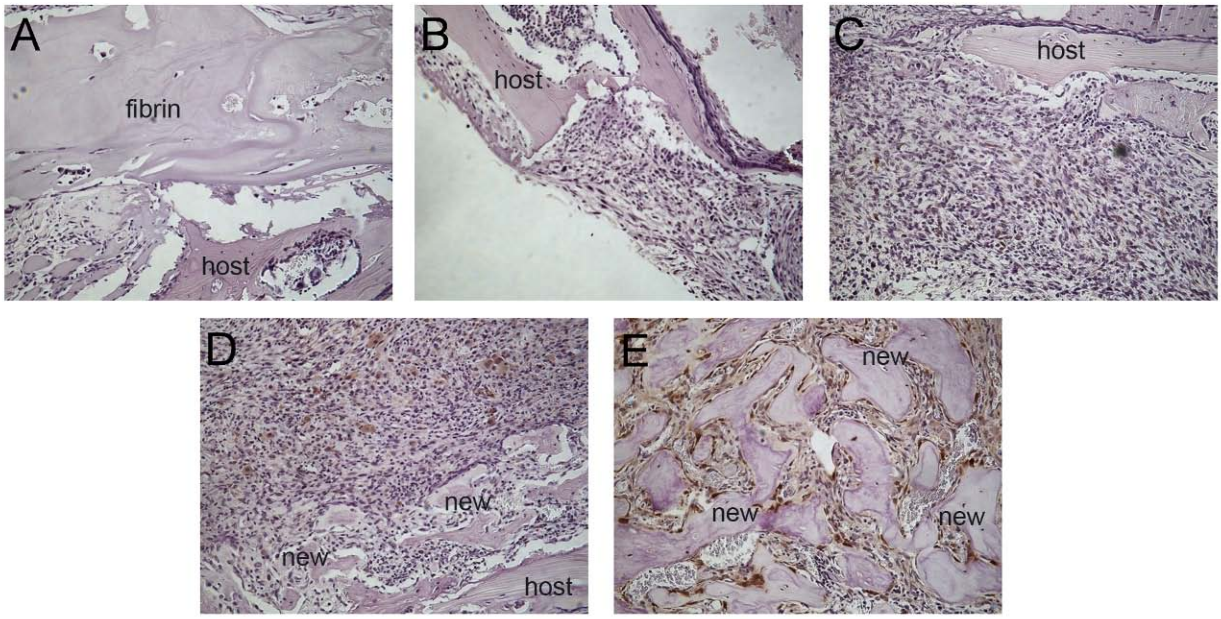

Figure 18: GFP staining of cranial defect healing in male hosts

Representative images of GFP staining of cranial defect in male hosts at A) 2 days B) 4 days C) 7 days D) 10 days E) 28 days post treatment with MDSC-B4. All images 200x. fibrin- fibrin scaffold, host- host bone, new- new bone tissue

In castrated male hosts, tracking of donor cells reveals similar patterns to unaltered male hosts. Donor cells are observed as small, rounded mononuclear cells scattered throughout the defect area at 2, 4 and 7 days post treatment. At 10 days post treatment, unlike unaltered male hosts, large, flat donor cells are not observed; donor cells that are present still maintain a small, rounded phenotype. At 14 days post treatment, donor cells are discerned as both chondrocytes and osteoblasts, and at 28 days, osteoblasts and osteocytes of donor origin are scattered among the bone tissue covering the defect.

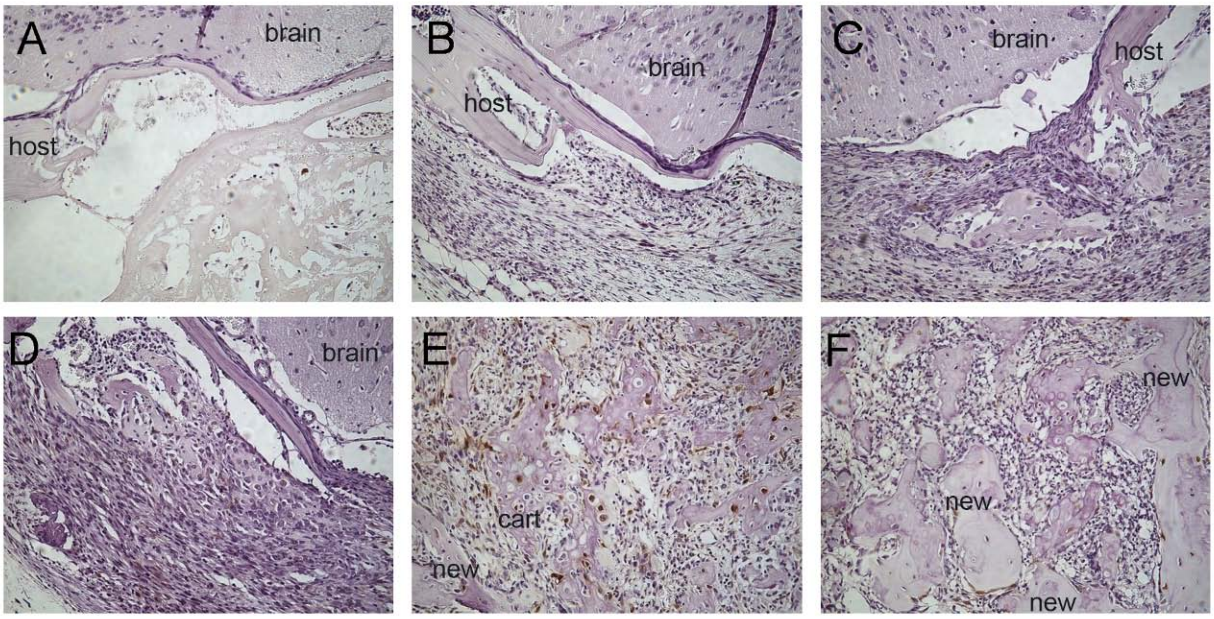

Figure 19: GFP staining of cranial defect healing in castrated hosts

Representative images of GFP staining of cranial defect in castrated hosts at A) 2 days B) 4 days C) 7 days D) 10 days E) 14 days and F) 28 days post treatment with MDSC-B4. All images 200x. host- host bone, new- new bone tissue, brain- host brain

Similar to unaltered and castrated male hosts, in unaltered female hosts, donor cells are also observed throughout the bone formation and defect healing process. However, in female hosts, the contribution of donor cells to new tissue is different from male hosts. At 2 and 4 days post treatment, donor cells are again small, round and mixed with host cells. However, at 7 and 10 days post treatment, and especially at 14 days, donor cells are observed in the flat, large phenotype. At 14 days, some donor cells are also noted as chondrocytes and osteoblasts. At 28 days post treatment, although the bone tissue formed is not as mature as in unaltered or castrated male hosts, donor cells are participating as osteoblasts and osteocytes in bone and chondrocytes in cartilage.

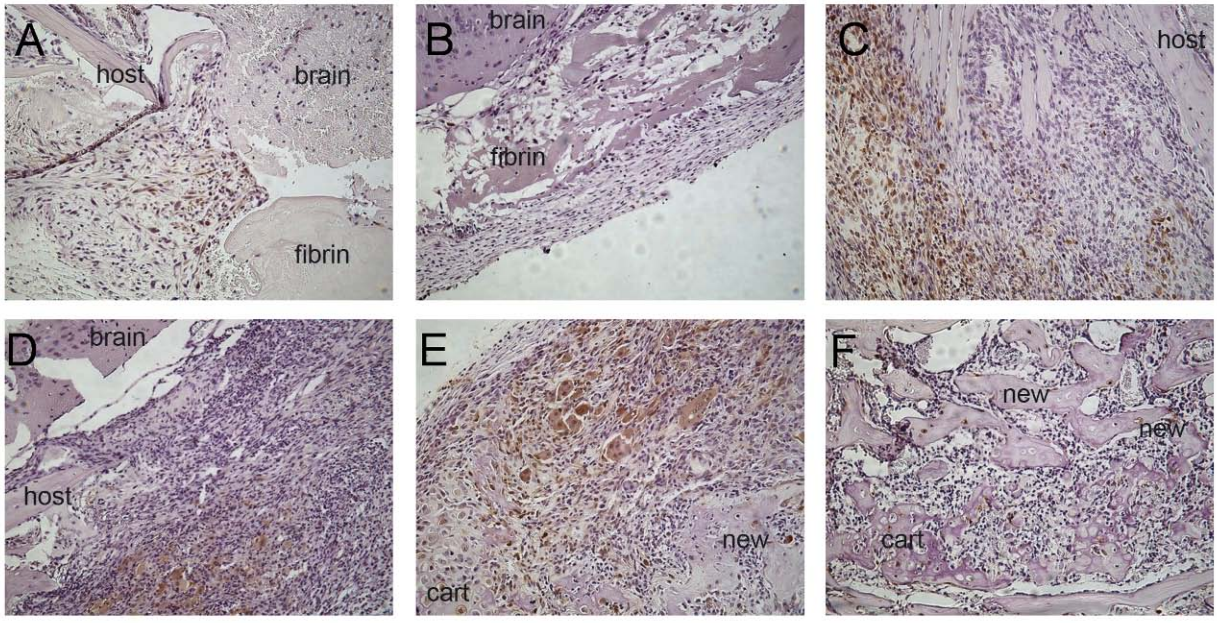

Figure 20: GFP staining of cranial defect healing in female hosts

Representative images of GFP staining of cranial defect in female hosts at A) 2 days B) 4 days C) 7 days D) 10 days E) 14 days and F) 28 days post treatment with MDSC-B4. All images 200x. fibrin- fibrin scaffold, host- host bone, new- new bone tissue, brain- host brain, cart- cartilage

Donor cells in ovariectomized hosts are similarly distributed to those in unaltered female hosts: small, rounded donor cells are found at 2, 4 and 7 days post treatment, while at later time points, like 14 days, large and flat donor cells are observed. Like all other groups, at 28 days post treatment, donor cells are contributing to all aspects of the bone formed as chondrocytes, osteoblasts and osteocytes.

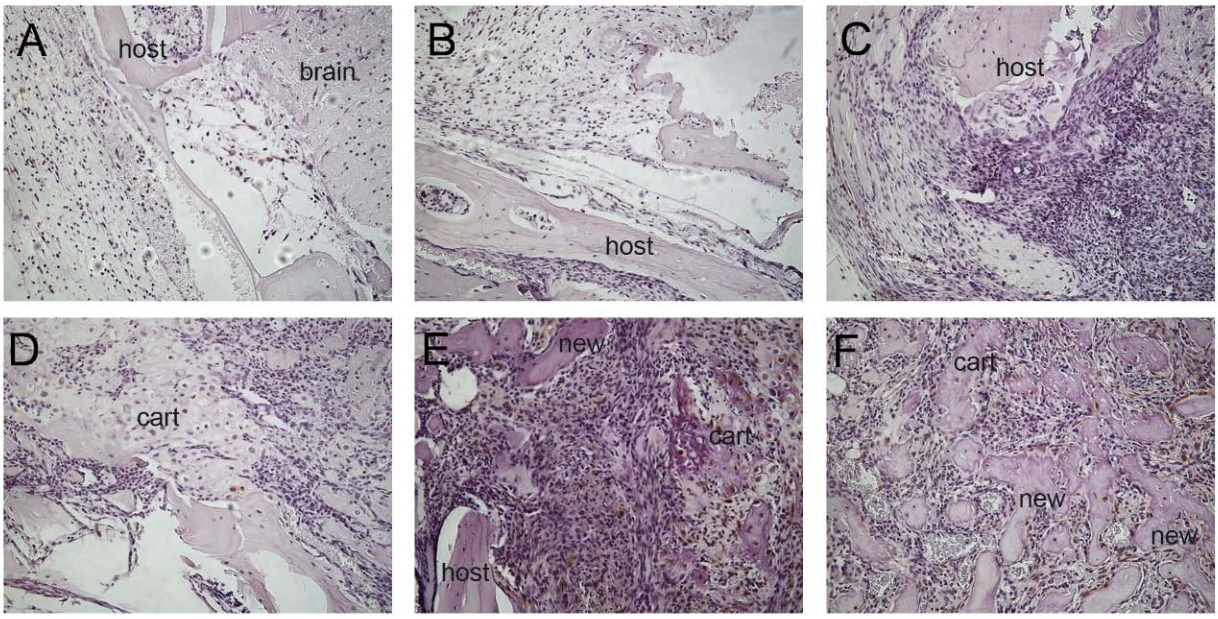

Figure 21: GFP staining of cranial defect healing in ovariectomized hosts

Representative images of GFP staining of cranial defect in ovariectomized hosts at A) 2 days B) 4 days C) 7 days D) 10 days E) 14 days and F) 28 days post treatment with MDSC-B4. All images 200x. host- host bone, new- new bone tissue, brain- host brain, cart- cartilage

3.4 DISCUSSION

In order to determine if host sex and/or sex hormones affect bone repair, MDSC-mediated healing of a cranial defect was evaluated in unaltered male, castrated male, unaltered female and ovariectomized female hosts. Increased bone formation at the callus site of a long bone fracture has been correlated to fracture healing [100]. Since increased MDSC-mediated ectopic bone formation was seen in male hosts compared to female hosts, it was theorized that healing of a bone fracture or defect may also be accelerated in male hosts compared to female hosts. In this bone healing study, as in ectopic bone formation studies, differences were found between male and female hosts. However, unlike ectopic bone formation studies, some measures were also different between hosts of the same sex: male and castrated male or female and ovariectomized female.

One measure to quantify healing of the calvarial defect is planar defect area. This measure was used by our group in previous studies evaluating the efficacy of MDSC therapies because radiography was the only non-histological means of quantifying bone repair at that time [8, 101]. Presently, microCT is available to our research group, so three dimensional reconstructions were rendered as two dimensional images and evaluated as two dimensional radiographs were previously assessed. At 28 days, all defects in all groups (unaltered male, castrated male, unaltered female, ovariectomized female) were completely healed with defect area equal to zero, and therefore, only 14 day defect areas were compared. Only between ovariectomized female and castrated male host groups were the defect areas significantly different; however, a trend of larger defect size in ovariectomized hosts compared to unaltered male or female hosts was also observed. Defect size remaining is inversely related to healing of the cranial defect; that is, larger defect size indicates less healing. From planar area

measurements, it can be concluded that ovariectomized females healed the least at 14 days post treatment.

Using microCT measurements, the volume of bone formed within the defect and the volume of total bone formed were calculated. Less healing was also observed in ovariectomized groups when examined within defect bone volume at 14 days, with a trend of less within defect bone when compared to the other three host groups. While all groups significantly increase within defect bone volume from 14 days to 28 days, unaltered females and ovariectomized females form less within defect bone at 28 days when compared to castrated males.

At 14 days, ovariectomized host animals display significantly smaller total bone volume than castrated hosts, and ovariectomized hosts also exhibit a trend of smaller total bone volume than unaltered male or unaltered female hosts. At 28 days, total bone volumes show the following trend from largest total bone volume to smallest: unaltered male, castrated male, unaltered female, ovariectomized female. Ovariectomized hosts exhibit significantly less total bone than both unaltered male and castrated male hosts, and unaltered female hosts show significantly less total bone formed than unaltered male hosts.

Overall, trends and significant differences observed in within defect and total bone volume are similar to ectopic bone studies in Chapter 2. However, in this healing study, unlike ectopic bone studies, all male hosts (both unaltered and castrated) were not always significantly different from all female hosts (both unaltered and ovariectomized) suggesting that sex hormone differences due to castration or ovariectomy may play a role in bone healing that was not noted in ectopic bone formation studies. Intramuscular ectopic bone formation, while providing a fast and valuable measure of the efficacy of osteogenic capacity of cells, materials, and other therapies, is at its core, a false system. Unlike developmental bone formation or long bone

fracture healing, in ectopic bone formation assays, the endochondral bone formation cascade is brought about by extrinsic osteogenic factors (cells, proteins, or biomaterials) not normal developmental or healing signals. While these factors can, in fact, bring about ectopic bone formation, a bone healing research model provides more information as to clinical efficacy of osteogenic therapies. If one were to consider only the ectopic bone studies of Chapter 2, castration and ovariectomy appear to have no effect; however, in bone healing studies of Chapter 3, animals which are surgically castrated or ovariectomized behave differently. Relying only on ectopic bone formation assays to determine the utility of osteogenic therapies should be avoided; bone healing models, both long bone and craniofacial, should also be considered.

Because it was evident that the bone formed at the defect site was not at the proper location, spatial control index was also calculated. This spatial control index was defined as (within defect bone volume/ total bone volume * 100%), and a spatial control index of 100% would indicate that all of the bone formed was located inside the defect. However, a spatial control index of 100% does not necessarily mean that the defect is 100% healed; it only means that the bone that did form was inside the defect. At 14 days, spatial control index calculated for both unaltered female and ovariectomized female hosts was significantly larger than the spatial control index calculated for castrated male hosts, indicating that in both types of female host a larger ratio of bone formed inside the defect to total bone formed. At 28 days, spatial control index decreased in all host groups. Ovariectomized female hosts display the largest spatial control index, and this is significantly different from the spatial control index of unaltered male or unaltered female hosts at 28 days. From 14 to 28 days, spatial control index in all groups decreases by approximately a factor of ten; this is not due to less bone forming within the defect area over time, but instead because the total volume of bone formed increases so dramatically

(see Figure 13). Within defect bone volume increases for all groups from 14 to 28 days; it just does not increase as rapidly as total bone volume. While this spatial control index computation does not describe how the defect is healed, it does indicate that for all groups, the majority of the new bone is not in the correct location. These observations, combined with three dimensional reconstructions, indicate that instead of defect healing, this process is actually MDSC-mediated bone formation at the defect site.

In order to further examine differences in bone healing between the four host groups, H&E staining, as well as GFP immunostaining for identification of donor cells, were performed. Similar to ectopic bone studies, male hosts (both unaltered and castrated) displayed more mature bone tissue than female hosts (both unaltered and ovariectomized) at earlier time points. These histological analyses also further support that bone formation and not bone defect healing is what is occurring at the cranial defect site. Upon histological examination in all groups, endochondral bone formation is taking place, not intramembranous bone healing as would normally occur in cranial bone defects. Condensation of large groups of cells, chondrocyte maturation followed by remodeling, and mineralization of matrix all occur in this cranial defect model in the same manner as occurred in MDSC-mediated endochondral ectopic bone formation model. Moreover, it is apparent that this ectopic bone, while covering and filling the defect, does not integrate with the native bone on the edge of the defect. In all histological analyses, hosts of the same sex (unaltered and castrate male or unaltered and ovariectomized female) do not display obvious differences in tissue that could account for variations reported with quantitative microCT measures.

From H&E staining of samples of all groups, it can be concluded that the process that is occurring at the cranial defect site is actually MDSC-mediated endochondral bone formation, not

healing of the cranial defect. As in ectopic bone formation studies, H&E staining revealed that unaltered male and castrated male hosts undergo endochondral ossification more rapidly than unaltered female or ovariectomized hosts (see Figure 14, Figure 15, Figure 16, Figure 17). Male hosts (unaltered and castrated) display bone at 10, 14 and 28 days following treatment, while female (unaltered and ovariectomized) hosts have cartilage present at all of these time points. Again, similar to ectopic bone formation studies, an accelerated turnover from cartilage to bone is noted in male hosts, when compared to female hosts, in this critical size cranial defect model.

From GFP immunostaining for donor cells, it is also determined that in all host groups the majority of bone tissue is derived from host cells (see Figure 18, Figure 19, Figure 20, Figure 21). GFP immunostaining also further emphasizes the segregation of native bone at the defect edge and new bone containing MDSC-B4 cells. These MDSC-B4 cells are never observed adjoining native uninjured tissue; they are only present in the newly formed, non-integrated endochondral bone in all groups. The delay in endochondral bone formation in female hosts (both unaltered and ovariectomized) is highlighted by GFP immunostaining also. During the endochondral bone formation process, chondroprogenitor cells emerge from condensations of mesenchymal cells and then mature into hypertrophic chondrocytes. In female hosts, large flat donor cells are observed at 14 days (see Figure 20E, Figure 21E), and these are suspected to be chondroprogenitors in intermediate stages of differentiation. This phenotype of cells is never observed in male hosts (unaltered or castrated) because in male host, cells participating, whether donor or host derived, are rapidly converted from chondroprogenitor stage to hypertrophic chondrocytes to mineralized bone matrix.

Some clinical evidence exists that sex may be a factor in fracture healing; however, these studies are usually prospective studies evaluating non-union as the outcome and do not examine

the rate of healing. Female sex is associated with increased risk of non-union in femoral, scaphoid and mandibular fractures [102-104]. No known studies have examined host sex or sex hormones in the context of a critical size cranial defect model. However, a few studies have investigated host sex and sex hormones in long bone fracture healing. In one such study, ovariectomized, Vitamin D-deficient female rats did not display altered long bone fracture healing when compared to unaltered, nutritionally sound female rats [105]. In contrast, another study demonstrates impaired fracture healing in ovariectomized female compared to unaltered female rats [106]. Complementary studies by one research group determined that the same femoral defect in male and female hosts produces non-union only in female rats [107], and this was explained as a quantitative but not qualitative differences in mesenchymal stem cells found in male and female hosts [108]. Quality or quantity of mesenchymal stem cells were not evaluated from host groups in this study, but it is known that the majority of the new bone formed is derived from host cells so donor mesenchymal stem cells could be a factor. While the study presented here does not demonstrate differences in bone defect healing between sexes, it does reveal host sex differences in the response to MDSC-B4 when applied as a bone healing therapy which is important for translational considerations. This study also shows that MDSCs, when transduced with a retrovirus encoding for BMP4, produce endochondral bone when applied to a critical size cranial defect.

3.5 CONCLUSIONS

The aim of this study was to determine the effect of host animal sex and sex hormones on bone healing mediated by MDSCs, and this was evaluated using a critical size cranial defect model

treated with MDSC-B4 in altered male, castrated male, unaltered female, and ovariectomized female hosts. Two hypotheses were tested: one, MDSC-mediated cranial defect healing would be superior in male compared to female host animals and two, castration and ovariectomy would not affect MDSC-mediated bone healing sex differences. Like previous ectopic bone formation studies, cranial defect healing was reduced in female hosts when compared to male hosts. While some quantitative differences were seen in defect healing in castrated and ovariectomized hosts compared to unaltered counterparts, the hypothesis that castration and ovariectomy negatively influence MDSC-mediated bone healing was not validated. Using planar area of defect measurements, it was determined that ovariectomized hosts maintained largest defect size, indicating least healing, at 14 days following MDSC-B4 treatment. The total volume of bone formed, from greatest to least, in unaltered male, castrated male, unaltered female, and ovariectomized female hosts. However, spatial control index measurements and three dimensional reconstructions show that in all groups, the majority of the bone is forming on top of, rather than within, the cranial defect. Histological analyses show that this bone forming is actually endochondral bone, and not intramembranous bone as normally occurs in flat bone healing. While endochondral bone formation is not the desired outcome in craniofacial bone healing, the new bone tissue formed did in fact cover the defect which could be an acceptable result. Most importantly, this study demonstrated host sex, and to some extent sex hormone, differences in MDSC-mediated bone therapy applied to a critical size cranial defect. Future studies will examine modulation of type of bone healing (endochondral vs intramembranous) to reach the desired outcome for bone defect therapies.

4.0 APPLICATION OF MDSCS TO AN ESTABLISHED NON-HEALING DEFECT

4.1 INTRODUCTION

MDSCs have previously been studied as a means of healing critical size cranial defects; when applied at the time the defect is created, retrovirally transduced MDSCs can mediate healing of the defect [8, 101]. However, if MDSCs are used as a clinical therapy, application at the time of creation of a defect may not always be possible. Two situations that could possibly require delayed applications of MDSCs are atrophic long bone non-unions and craniofacial defects. A mouse model of long bone non-union was attempted (see Appendix), but a reproducible, effective model was not achieved. Therefore, a calvarial non-union (critical size cranial defect) was used in this study. A cranial defect was created in unaltered male mice and allowed to follow normal course of healing for three weeks; during this time the cranial bone does not repair, but instead the defect area becomes filled with fibrous, scar-like tissue. A second surgery was performed to treat the defects with three therapy groups: fibrin only, MDSCs in fibrin, and MDSC-B4 in fibrin, and all groups were evaluated with microCT and histological analyses. The hypothesis of this study was that MDSCs, when applied to a fibrous tissue filled non-healing bone defect, will induce healing in a manner similar to MDSCs applied at the time of creation of the defect.

4.2 METHODS

4.2.1 MDSC Isolation and Retroviral Transduction

Cells were isolated, cultured, retrovirally transduced and stored in the same manner as described in section 2.2.1.

4.2.2 Surgical Procedure

For this study, unaltered male were purchased from Jackson Laboratories, and surgeries were performed at age 12 weeks. Following sterile surgical procedures outlined in the University of Pittsburgh IACUC Protocol #1003499, each animal was anesthetized and an incision was made along the frontal and parietal bones of the skull. To create the critical size cranial defect, the scalp was dissected and 5 mm trephine was used to create the circular bone defect. The incision was then closed with sutures and the animals were allowed to resume normal activity. After three weeks, the animals were anesthetized again for a treatment surgery. A similar incision was used, and obvious thickened fibrous tissue was removed from the defect area; however, even with a stereomicroscope, it was difficult to physically separate fibrous tissue from intact dura and only a small amount of tissue was removed from each animal. Just prior to treatment, 100,000 MDSC-B4 or MDSC-G were mixed with sealer protein solution, and this mixture was applied to the defect simultaneously with thrombin solution. The sealer and thrombin solutions are components of Tisseel fibrin sealant kit (Baxter Biosurgery), and total volume was ~40uL of fibrin. The secondary treatment incisions were then closed with sutures and the animals were allowed to resume normal activity. Animals were sacrificed at various time points following treatment: 2, 4,

7, 10, 14 and 28 days. A separate group had the critical size cranial defect created, but never treated; these animals were analyzed to follow the normal non-healing process of the defect. Each group was made up of 9-13 animals for microCT analysis, in addition to animals designated for histological analysis.

4.2.3 microCT Analyses

Healing of the critical size cranial defect was monitored in all groups with a microCT scanner (VivaCT40, Scanco Medical) at 2 and 4 weeks post treatment (noted as 3wk + 2wk and 3wk + 4wk). Mice were anesthetized and positioned in an animal scanning bed with the skull in specially designed holder. Scanning was performed with the following settings: energy of 55 kVp, intensity of 145 μA, nominal resolution of 35 μm, and integration time of 200 ms. Two-dimensional image slices were obtained and contour lines were drawn to define volume of interest (VOI). An appropriate threshold was chosen for the bone voxels by visually matching thresholded areas to grayscale images. The threshold was kept constant throughout the analyses. This led to a three-dimensional reconstruction of the ectopic bone and provided quantitative data on bone volume (mm^3).

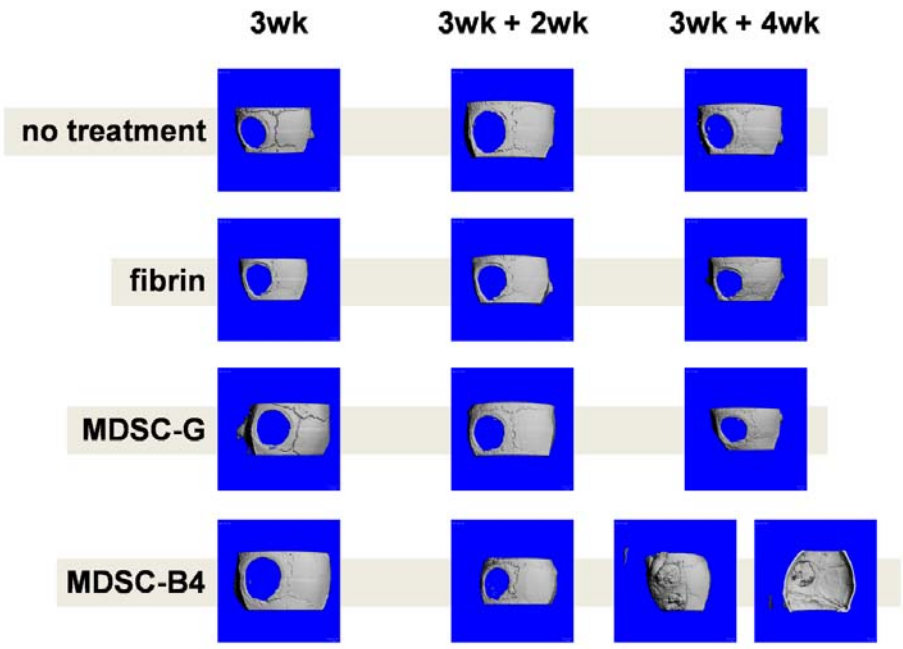

Figure 22: Representative microCT reconstructions of cranial defects

As previously described in 3.2.3, in order to compare with previous studies which quantified non-healed area of defect from planar radiographs, three-dimensional reconstructions were analyzed using Northern Eclipse imaging software. First, a calibration of pixel number to distance on the scale bar generated on the three-dimensional reconstruction was performed. Then, the image was changed to grayscale and thresholds were applied to determine the area of the region selected (see Figure 10). Planar area of defect was computed for every animal in each host group (9-13 animals) at three weeks following creation of defect (3wk) and two and four weeks following treatment (3wk+2wk and 3wk+4wk, respectively), and resulting data are displayed as mean ± standard deviation.

In addition to defect area measurements, volume measurements were computed for both total new bone formed, as well as bone formed within the defect (see Figure 11). For each two-dimensional slice, areas encompassing all bone formed (including rounding and healing of defect

margins) were drawn. Volume of total new bone was the computed for each sample (9-13 animals per group) at three weeks following creation of defect (3wk) and two and four weeks following treatment (3wk+2wk and 3wk+4wk, respectively). Later, total new bone volume areas drawn on each slice were edited and modified to only include new bone formed within the defect (including rounding and healing of defect margins, but only to the thickness of native skull). From these areas, volume of within defect bone formed was computed for each sample. All volume data are displayed as mean ± standard deviation.

Spatial control index of bone formation was also calculated, and it is defined as (within defect bone volume/ total bone volume) *100%. Therefore, a spatial control index of 100% would indicate that all bone formed during the healing process was formed only within the cranial defect.

4.2.4 Histological Analyses

After sacrifice of mice, the skull, with the mandible and skin removed, were placed in formalin (3.7% neutral buffered formaldehyde) for 24 hours. The samples were then decalcified in 10% EDTA (Sigma-Aldrich). Dehydration and then paraffin embedding followed, and samples were cut into 5 micron sections and dried.

Following deparaffinization and rehydration, sections of bone containing the defect area were stained using standard procedure for hematoxylin and eosin staining (H&E) to determine general tissue morphology. Donor cells were distinguished from host cells by staining for GFP, since all donor cells produce GFP and BMP4 or GFP only. Briefly, after blocking in both 3% H_2O_2 in methanol and 2% horse serum in PBS, biotintylated anti-GFP antibody (Vector Laboratories) was applied at a 1:1000 dilution. Then, streptavidin/HRP (R&D) was applied at a

1:50 dilution followed by DAB Peroxidase Substrate Kit (Vector Laboratories) per manufacturer's instructions. Hematoxylin QS (Vector Laboratories) was used as a counterstain. Resultant stain shows donor cells expressing GFP (MDSC-B4) as brown and all cells from the host as purple.

All images were taken on Nikon Eclipse E800 microscope equipped with a Retiga EXi digital camera using QCapture software for brightfield images.

4.2.5 Statistical Analysis

All numerical values (planar area, within defect volume, total volume, spatial control index) were computed using microCT measurements from 9-13 animals per group: no treatment, fibrin, MDSC-G and MDSC-B4. Statistical analyses (ANOVA or repeated measures ANOVA) were performed with SPSS, and differences were considered significant if $p<.05$.

4.3 RESULTS

A critical size cranial defect was created in male mice and allowed to follow the normal course of healing for three weeks, when the defect had filled with fibrous scar tissue. Following this healing period, three different treatments (fibrin only, MDSC-G, or MDSC-B4) or no intervention were applied to the defect area. Using microCT scanning and histological analyses, differences in cranial bone healing between the four groups were observed.

4.3.1 Planar Area of Defect

Following microCT scanning, a three-dimensional reconstruction of each defect area was created, and this reconstruction was the processed to determine the area of the defect remaining at three weeks following creation of defect (3wk) and two and four weeks following treatment (3wk+2wk and 3wk+4wk, respectively). At three weeks, all groups displayed similar defect area, as expected since no groups had received treatment at this time point. Following two weeks of treatment, MDSC-B4 and fibrin groups had decreased defect area significantly, indicating healing in these groups. Following four weeks of treatment, MDSC-B4 group continued to heal and demonstrated significantly smaller defect area than all other groups, indicating superior healing in MDSC-B4 group. Also of note, two animals (of ten) in MDSC-B4 group displayed a defect area of $0mm^3$ following four weeks of treatment, indicating that the defect was completely covered with new bone in these animals.

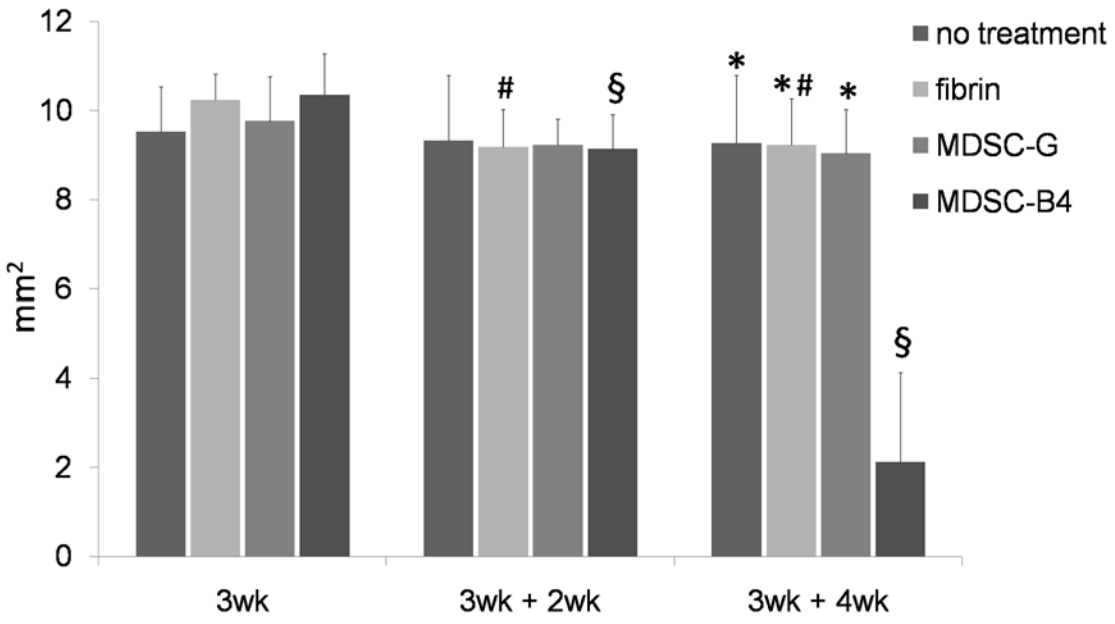

Figure 23: Planar area of defect

Area of defect (mm^3) at 3 weeks following defect creation, after 2 weeks of treatment and after 4 weeks of treatment. All statistical notations indicate $p<.05$. § from MDSC-B4 at 3 weeks, # from fibrin at 3 weeks, * from MDSC-B4 at 3 weeks + 4 weeks treatment.

4.3.2 Bone Volume Formed after Treatment

Within defect bone volume and total bone volume formed were quantified for at three weeks following creation of defect (3wk) and two and four weeks following treatment (3wk+2wk and 3wk+4wk, respectively). All groups formed a small amount of bone within the defect area, but only MDSC-B4 animals increased this amount from two to four weeks post treatment. MDSC-B4 animals also demonstrated significantly more within defect bone volume than other groups at four weeks post treatment. Total bone volume at two weeks post treatment was similar in all

groups; however, at four weeks post treatment, the MDSC-B4 group significantly increased over two week volume and also was significantly larger than other groups at four weeks post treatment.

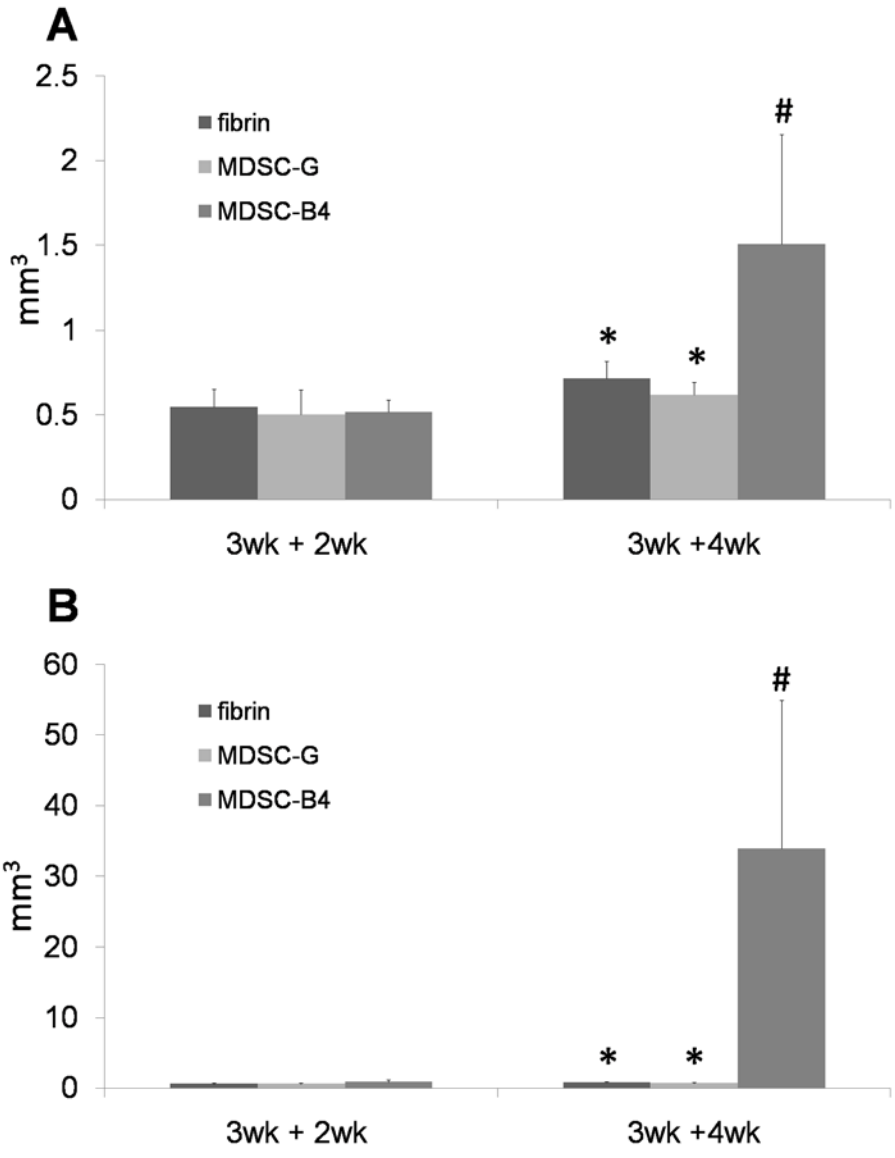

Figure 24: Within defect and total new bone volume

A) Within defect bone volume (mm^3) after two and four weeks of treatment with fibrin, MDSC-G and MDSC-B4. B) Total new bone volume (mm^3) after two and four weeks of treatment with fibrin, MDSC-G and MDSC-B4. All

statistical notation indicate p <.05. # MDSC-B4 at 3 weeks + 2 weeks treatment, MDSC-B4 at 3 weeks + 2 weeks treatment.

4.3.3 Spatial Control Index of Defect Healing

When examining the three-dimensional reconstructions, as well as within defect and total bone volumes, it was evident that not all bone formed is located within the defect area. The majority of the bone tissue formed is on top of the skull, covering but not filling the defect. A measure of spatial control index (within defect bone volume/ total bone volume *100%) was computed for each group at two weeks and 4 weeks post treatment. While both fibrin and MDSC-G groups maintain the same spatial control index (both relative to other and also over time), the MDSC-B4 treatment group demonstrates significantly lower spatial control index at two weeks post treatment, and this spatial control index plummets as treatment period goes to four weeks. At four weeks post treatment, only 5.58% of total bone formed in the MDSC-B4 group is within the defect area.

Table 2: Spatial Control Index of Bone Formation by Treatment Group

	fibrin	**MDSC-G**	**MDSC-B4**
3wk + 2wk	89.97% #	85.21% #	64.83%
3wk + 4wk	91.23% *	89.93% *	5.58% #

All symbols indicate p<.05. # MDSC-B4 at 3 weeks + 2 weeks treatment, MDSC-B4 at 3 weeks + 2 weeks treatment.

4.3.4 Histological Analyses

H&E staining and GFP immunostaining were performed on sections of each group at various time points to evaluate healing of the defect and monitor tissue contribution of both donor and host cells.

4.3.4.1 H&E Staining

Critical size cranial defects, when left untreated, are healed by a covering of fibrous tissue instead of repaired bone tissue filling the defect. These representative images of H&E staining of an untreated critical sized cranial defect demonstrate this fibrous covering, as well as the rounding of the edges of the bone defect over time.

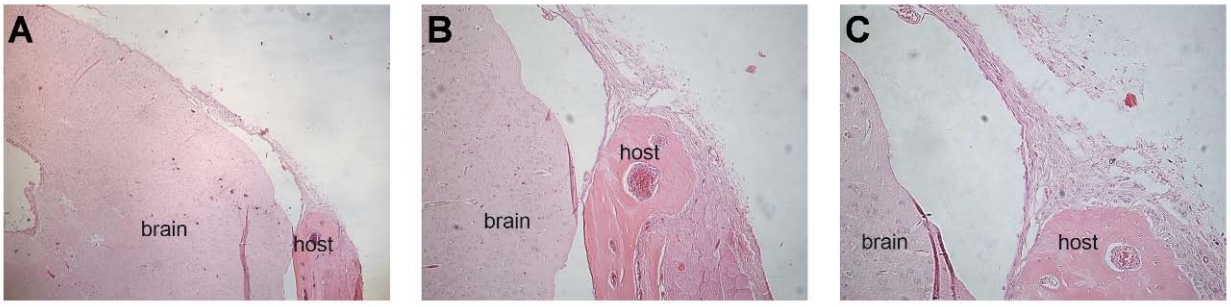

Figure 25: H&E staining of untreated critical size cranial defects

Representative images of H&E staining of untreated cranial defects at 7 weeks after creation of the defect.

A) 40x B) 100x and C) 200x. brain- host brain, host- host bone

In critical size cranial defects that are treated with a delayed application of fibrin, similar healing patterns are seen to fibrin only treatment. Representative H&E staining images depict an acute host response followed by fibrous tissue filling the defect.

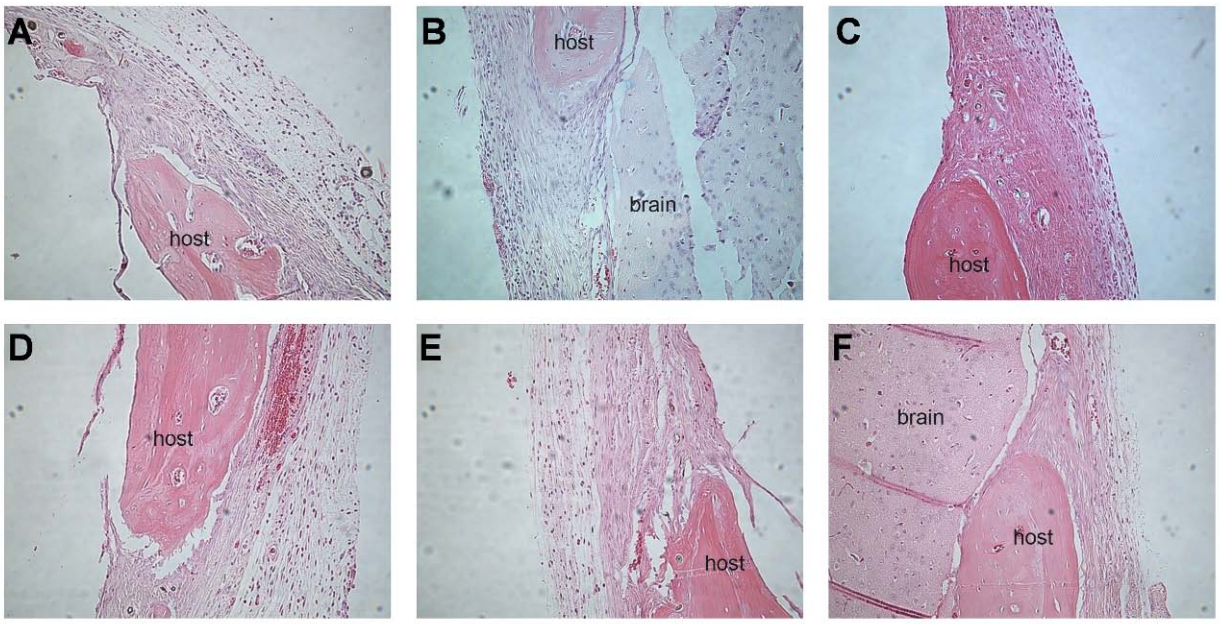

Figure 26: H&E staining of critical size cranial defect following delayed application of fibrin

Representative images of H&E staining of critical size cranial defects following delayed application of fibrin. Time points indicate time following three weeks of healing time. All images 200x. A) 3wk +2d B) 3wk + 4d C) 3wk + 7d D) 3wk +10d E) 3wk + 2wk F) 3wk + 4wk. host- host bone, brain- host brain

In critical size cranial defects that are treated with a delayed application of MDSC-G in fibrin, similar healing patterns are seen. Representative H&E staining images again show an acute host response to fibrin treatment, eventually followed by fibrous tissue filling the defect (Figure 27).

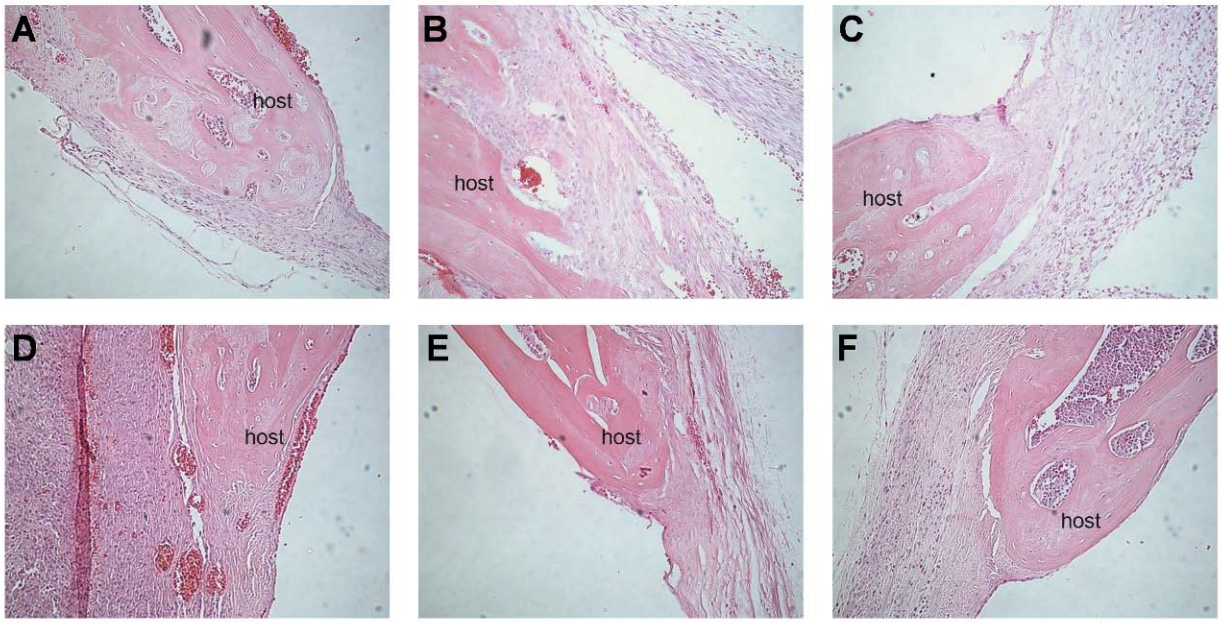

Figure 27: H&E staining of critical size cranial defect following delayed application of MDSC-G

Representative images of H&E staining of critical size cranial defects following delayed application of MDSC-G. Time points indicate time following three weeks of healing time. All images 200x. A) 3wk +2d B) 3wk + 4d C) 3wk + 7d D) 3wk +10d E) 3wk + 2wk F) 3wk + 4wk. host- host bone

In critical size cranial defects treated with a delayed application of MDSC-B4 in fibrin, completely different results are found. At 10 days following treatment, the processes of endochondral ossification begins, and at 14 days, bone starts to appear over the defect area. At 28 days post treatment, all cartilage has been remodeled into bone; however, this new bone is not integrated with the edges of the defect. The fibrous tissue covering the defect remains unchanged throughout the bone formation process.

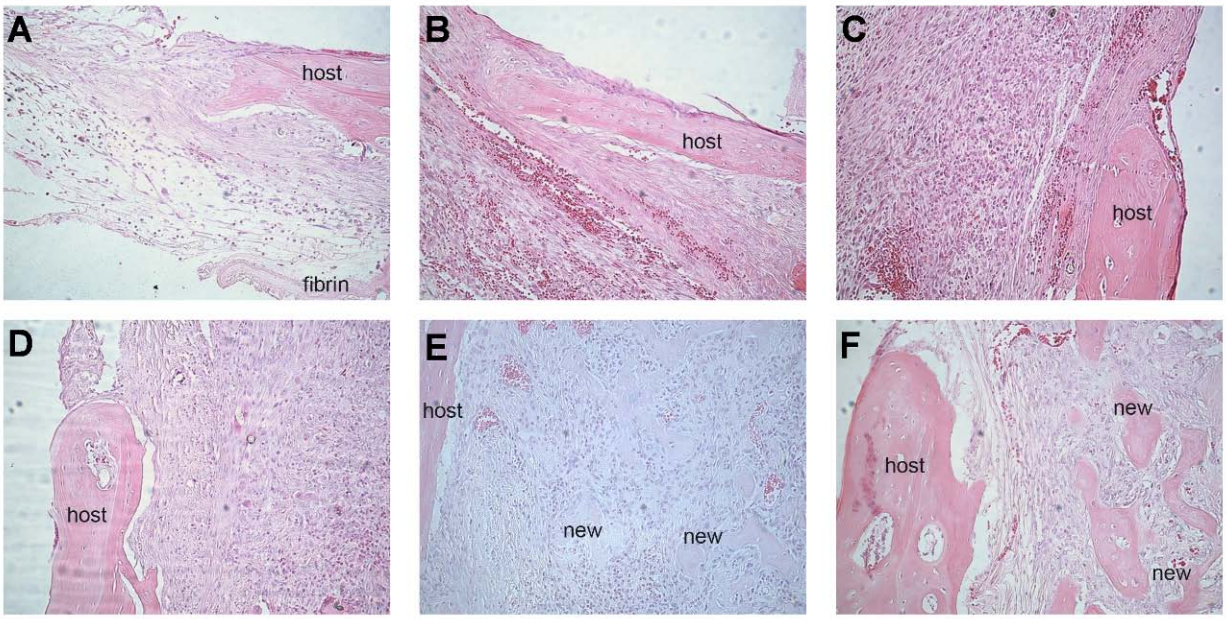

Figure 28: H&E staining of critical size cranial defect following delayed application of MDSC-B4

Representative images of H&E staining of critical size cranial defects following delayed application of MDSC-B4. Time points indicate time following three weeks of healing time. All images 200x. A) 3wk +2d B) 3wk + 4d C) 3wk + 7d D) 3wk +10d E) 3wk + 2wk F) 3wk + 4wk. host- host bone, fibrin- fibrin scaffold, new-new bone

4.3.4.2 Identification of Host and Donor Cells

Using a peroxide-based staining kit and an anti-GFP antibody, donor cells (stained brown in images) were distinguished from host cells (stained purple in images). In MDSC-G treatment group, while donor cells were present at early time points following treatment (2 days, 7 days, 4 days) at later time points (10 days and on) no GFP positive donor cells are detected.

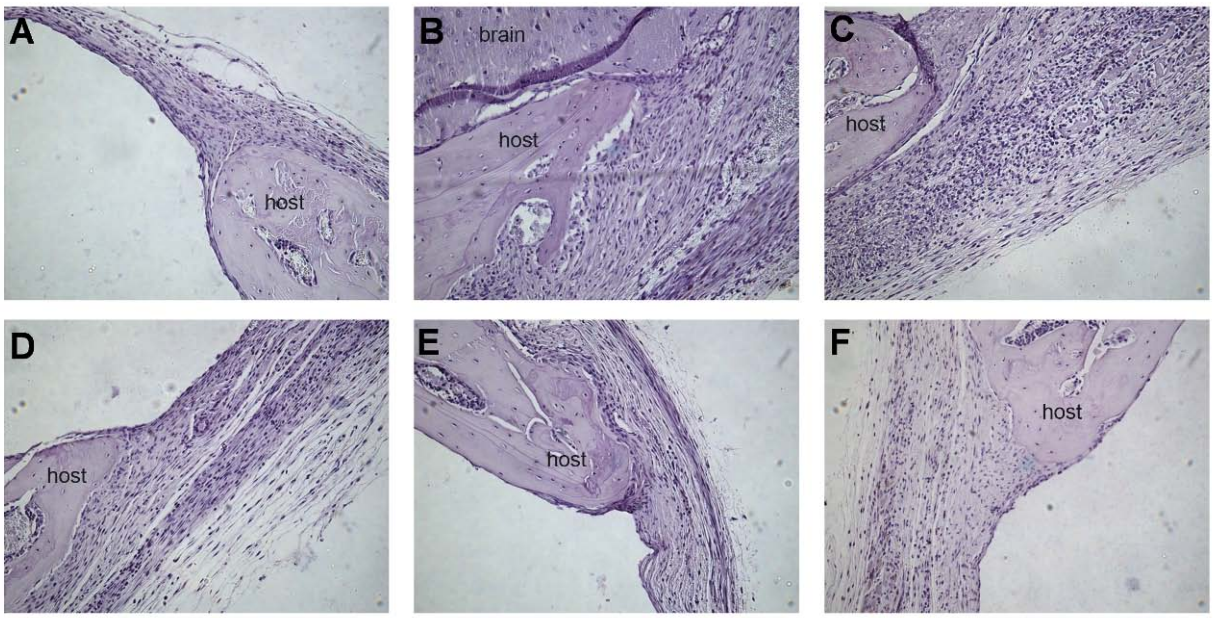

Figure 29: GFP immunostaining of critical size cranial defect healing following delayed application of MDSC-G

Representative images of GFP immunostaining of critical size cranial defects following delayed application of MDSC-G. Time points indicated time following three weeks of healing time. All images 200x. A) 3wk +2d B) 3wk + 4d C) 3wk + 7d D) 3wk +10d E) 3wk + 2wk F) 3wk + 4wk. host- host bone, brain- host brain

In MDSC-B4 treatment group, GFP-positive donor cells are present at all time points and contribute to new bone tissue formed through endochondral ossification. At 7 and 10 days following treatment, donor cells are observed as large, flat cells interspersed with many host cells. At 2 weeks following treatment, donor cells are mostly participating as chondrocytes, but at 4 weeks following treatment, donor cells are seen as chondrocytes, osteocytes and osteoblasts in all phases of endochondral ossification. The segregation of new bone tissue formed (containing donor cells) from host bone at the defect edges is also quite apparent at 4 weeks post treatment.

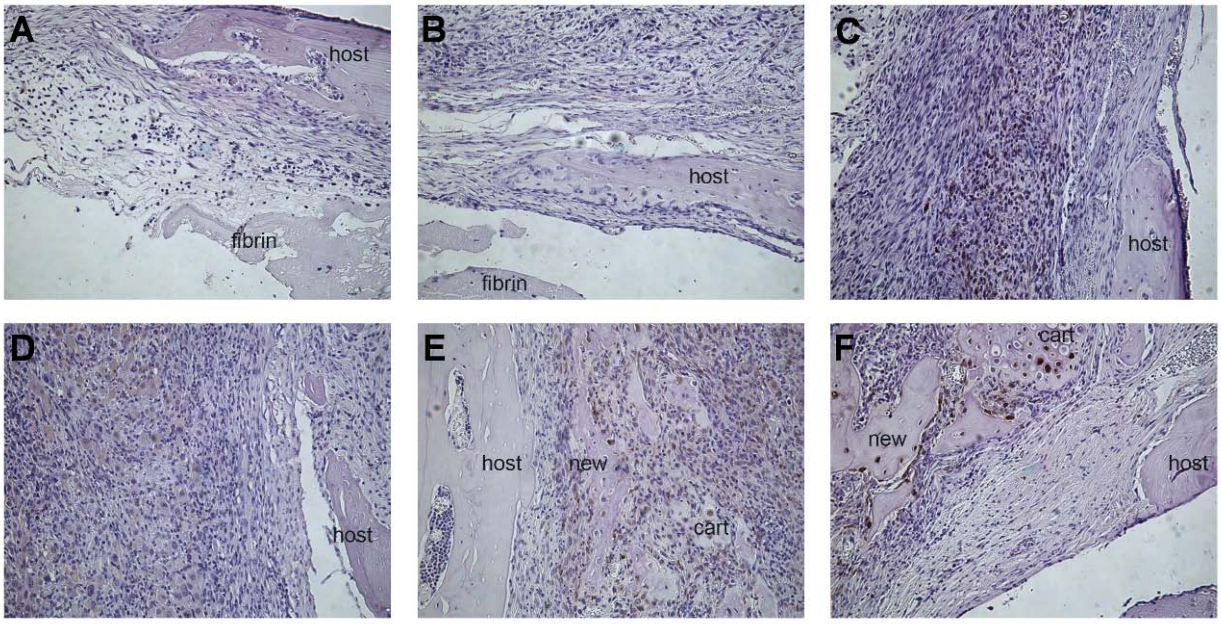

Figure 30: GFP immunostaining of critical size cranial defect healing following delayed application of MDSC-B4

Representative images of GFP immunostaining of critical size cranial defects following delayed application of MDSC-B4. Time points indicate time following three weeks of healing time. All images 200x. A) 3wk +2d B) 3wk + 4d C) 3wk + 7d D) 3wk +10d E) 3wk + 2wk F) 3wk + 4wk. host- host bone, fibrin- fibrin scaffold, new- new bone, cart- cartilage

4.4 DISCUSSION

In order to determine the efficacy of MDSC treatment in an established non-healing bone defect, a critical size cranial defect was created in mice. Animals were left untreated for three weeks, and during this time the defect filled with fibrous, scar-like tissue. After three weeks, treatment of either MDSC-G or MDSC-B4 in fibrin or fibrin alone was applied to the defect, and healing was evaluated via microCT and histological analyses.

Representative microCT reconstructions at two and four weeks post treatment, showed similar healing patterns among non-treated, fibrin only and MDSC-G groups. Little, if any, bone healing occured at the edge of the defect. In contrast, defects in the MDSC-B4 treated group are covered with some degree of new bone, and two of ten animals show complete covering of the defect. However, intracranial views of reconstructions in the MDSC-B4 group show that the bone covering the defect, is in fact, located on top of the defect and does not integrate with edges of the defect or non-injured cranial bone. After four weeks of treatment, defect margins are clear in intracranial views of all MDSC-B4 treated animals.

Similarity in healing among non-treated, fibrin only and MDSC-G groups was also demonstrated in planar defect area measurements; in MDSC-B4 treated animals, defect area is significantly smaller than in the other three treatment groups, indicating less defect remaining and therefore greater healing. Non-treated, fibrin only and MDSC-G groups displayed similar healing in three-dimensional microCT reconstructions; therefore, only treatment groups (fibrin and MDSC-G) were evaluated for bone volumes measurements.

Within defect bone volume was not significantly different in any groups following two weeks of treatment. However, after four weeks of treatment with MDSC-B4, this group demonstrated significantly larger within defect bone volume. Comparable volume measurements are seen when examining total bone volume also; MDSC-B4 treated animals display significantly higher total bone volume formed after four weeks of treatment than other groups. At two weeks, no differences are found in total bone volume between treatment groups. Another interesting observation is that neither MDSC-G nor fibrin only groups demonstrate an increase in within defect or total bone volume from two weeks to four weeks.

Another measurement of cranial defect healing was spatial control index. Here, the spatial control index was calculated as (within defect bone volume/ total bone volume * 100%), and a spatial control index of 100% indicates that all of the bone formed was located inside the defect area. However, a spatial control index of 100% does not necessarily mean that the defect was 100% healed; it only meant that the bone that was present is inside the defect area. From three dimensional reconstructions, it was apparent that the defect is not completely healed in MDSC-G or fibrin only groups; however, these groups have spatial control indices of approximately 90% at both two and four weeks post treatment, indicating approximately 90% of the small volume of bone that formed in these groups lied within the defect space. Spatial control index of MDSC-B4 treated group (64%) was significantly less than MDSC-G or fibrin only at two weeks post treatment. Most importantly, at four weeks post treatment with MDSC-B4, where the open defect is no longer visible, spatial control index decreases to 5% and this was significantly less than MDSC-G or fibrin only at four weeks post treatment and also MDSC-B4 at two weeks post treatment. This low spatial control index was due to the large total volume of bone formed, in relation to the amount formed in the defect, rather than a very small amount of bone formed in the defect location. Combining these data with the intracranial views of three dimensional reconstructions, it was apparent that the bone that is formed in MDSC-B4 treated animals is actually located above the defect and covered the defect, but does not fill it.

Histological analyses of all groups and time points were examined to better elucidate what is occurring at the defect site. First, with H&E staining, the morphological appearance of an untreated critical size cranial defect was examined seven weeks after it was created (Figure 25). With no intervention, the body heals a defect of this size by filling the volume with fibrous tissue. After seven weeks, this fibrous tissue is continuous with the periosteum of the

surrounding bone and no inflammatory or injury response is noted; the defect appears to be biologically inactive.

In animals that received fibrin treatment three weeks after defect creation, the final appearance, at seven weeks post defect creation, was similar. The short-term effects of fibrin treatment were observed in the host as an infiltration of host cells to the defect site, followed by degradation of fibrin, and disappearance of infiltrating cells. Response in MDSC-G treated groups was comparable: host response to fibrin, followed by fibrin degradation, and finally the defect area became filled with fibrous tissue. These observations lead to the conclusion that in a critical size cranial defect, delayed treatment with fibrin or MDCS-G was equivalent to no treatment when examined at later time points.

MDSC-B4 treatment appears to elicit positive response for defect healing when examining three dimensional reconstructions or bone volume measurements. However, upon histological examination with H&E staining, it became apparent that the bone tissue that forms at the defect site was created through endochondral ossification, not intramembranous ossification that is typical in cranial bone healing. Early time points following MDSC-B4 treatment (2, 4 and 7 days post treatment) were similar to other groups with an infiltrative host response and degradation of fibrin observed. At 10 days post treatment, cartilage was observed, and at 14 days post treatment this cartilage tissue was remodeling into immature bone. At 28 days post treatment, mature trabecular bone was observed at the defect site. However, this newly formed bone did not integrate with native bone at the edges of the defect site or penetrate in to the fibrous tissue filling the defect; this new bone lied on top of the cranial defect like a hat. These histological observations confirmed observations from intracranial three dimensional

reconstructions that the defect was not filled with bone tissue, but rather covered by bone in MDSC-B4 treated groups following four weeks of treatment.

To determine the contribution of donor cells to bone tissue formed, immunostaining for GFP was performed. This stain was evaluated for both MDSC-G and MDSC-B4 groups. In the MDSC-G treated group, GFP positive donor cells are visible at 2, 4, and 7 days post treatment. These donor cells remain small and rounded, and their numbers decrease at 10 days. By 14 and 28 days post treatment, no donor cells were found. This is not surprising, as no additional bone is formed by MDSC-G treated groups over fibrin treatment or no treatment. If the MDSC-G donor cells are not contributing to any additional healing, perhaps the reason is because they do not remain in the tissue at later time points. In the MDSC-B4 treated group, donor cells persist and were present in all stages of endochondral bone formation. At early time points, like 2 and 4 days post treatment, MDSC-B4 GFP positive donor cells were observed as small, rounded cells interspersed with many infiltrating host cells. At 7 days post treatment, MDSC-B4 GFP positive donor cells were seen as large, flat chondroprogenitors, and at 10 and 14 days post treatment, these donor cells transformed into chondrocytes. At 14 and 28 days post treatment, MDSC-B4 GFP positive donor cells were contributing to endochondral bone tissue as chondrocytes, osteocytes, and osteoblasts. At 28 days, it was apparent that the new bone tissue formed, which contains GFP positive donor cells, was not integrated with the native bone tissue. The layer of fibrous tissue, made entirely of host cells, separated the new bone formed by MDSC-B4 and native bone.

The purpose of this study was to determine the efficacy of BMP4 retrovirally transduced MDSCs applied to an established non-healing bone defect. Ideally, a long bone non-union model would have been have been utilized, but this was not possible; therefore an untreated critical size

cranial defect (calvarial non-union) was studied. Results from this study must be carefully considered in the context of other studies. BMP proteins have previously been used to successfully heal bone in many orthopaedic and craniofacial bone defect applications; however, in most of these studies the BMP protein was applied to bone defects at or soon after creation [45, 109]. BMPs have also been previously used successfully when applied to established long bone non-unions [44, 46-49]. However, all of these clinical long bone non-union applications were preceded by debridement of soft tissue from the bone defect site.

Limitations due to the small size of the mouse model were encountered. During clinical treatment for a long bone non-union or non-healing craniofacial bone defect, typically the fibrous tissue filling the defect would be surgically excised before application of therapy [44, 46]. However, due to the thin nature of the dura in a mouse, the fibrous tissue, which filled the critical size cranial after three weeks of healing, could not be fully debrided without disturbing the dura and brain of the animal. Results of these studies could be affected by this limitation.

In this study, the target tissue for remodeling or healing was the fibrous tissue that filled the critical size defect over time. Fibroblasts have been previously used as cellular delivery vehicles for BMPs. Previous studies have shown that fibroblast-like cells from muscle, after transduction with retrovirus encoding for BMP4, can heal critical size cranial defects and segmental long bone defects [12, 101]. Primary fibroblasts have also been shown to undergo endochondral ossification following BMP4 retroviral transduction [52]. Moreover, other groups have shown BMP2 adenoviral transduced fibroblasts to be effective as therapy for cranial defects [110]. However, in this study, fibroblasts filling the bone defect remained unresponsive to BMP4 secreted by MDSC-B4 and no bone formed in the area of the fibroblasts.

The most important question remains: is bone covering the defect ultimately better than the fibrous tissue that would normally fill the defect if left untreated? The argument can be made that any bone covering a cranial defect is superior to a fibrous covering that could be penetrated by any mechanical assault. Future studies could involve biomechanical evaluation of this bone. Also, long term effects of this MDSC-B4 treatment were not evaluated to see how this endochondral bone remodels long term or if the bone formed by MDSC-B4 would eventually integrate with native bone.

4.5 CONCLUSIONS

The aim of this study was to determine the effect of MDSCs when applied to an established non-healing bone defect; the model used was an untreated critical size cranial defect in mice, and four groups were examined: no treatment, fibrin only, MDSC-G and MDSC-B4. The defect was created and allowed to follow the natural course of healing, wherein the defect filled with fibrous tissue, and after three weeks, the defect was then treated with the various therapies. The hypothesis was that MDSCs, when applied to a fibrous tissue filled non-healing bone defect, will induce healing in a manner similar to MDSCs applied at the time of creation of the defect. From microCT reconstructions and volume measurements it was determined that there was no difference among an untreated defect, a defect treated with fibrin and a defect treated with MDSC-G, and all of these groups showed minimal bone healing and similar fibrous tissue distribution in the defect. Animals that were treated with MDSC-B4 after the defect healed for three weeks did form new bone that covered the defect; however this bone was formed through endochondral ossification, not intramembranous bone healing, as would be expected in cranial

bone healing. Because the defect itself was not filled with newly formed bone, this outcome was determined to be dissimilar to treatment with MDSC-B4 at time of defect creation. Fibrous tissue located in the defect was not affected by MDSC-B4 application; this tissue looked histologically similar to the undisturbed fibrous tissue in non-treated animals. In summary, application of MDSC-B4 to an established non-healing cranial defect did bring about bone formation, which covered, but did not fill, the cranial defect. Future studies will examine means to modify this bone so the location and manner of formation will be more desirable.

5.0 SUMMARY AND FUTURE DIRECTIONS

MDSCs, due to their multipotent differentiation potential and ease of isolation, are an attractive cell source for stem cell based therapies in many tissues, including bone. Many questions must be answered before translation to clinical applications, even though MDSCs have been proven osteogenic both in vitro and in vivo, in both bone formation and bone healing models. In order for clinical therapies to be successful, they must be useful in many patient populations. The goal of this work was to determine the utility of MDSCs for osteogenic therapies in different hosts, each representing different patient groups. Differences in osteogenic capacity of MDSCs in both male and female hosts were examined because MDSCs are known to exhibit donor sex based differences in myogenic, chondrogenic, and osteogenic differentiation. Osteogenesis in ovariectomized and castrated hosts was also studied for two reasons: first, to determine the role of sex hormones in MDSC-mediated osteogenesis, and second, to provide insight into the role of MDSCs in aged hosts because ovariectomized and castrated animals are sometimes used to model age-related changes due to sex hormone status. Finally, MDSCs were examined in a cranial non-union to determine the utility of MDSCs in treating non-unions or defects with unfavorable host environments.

The first aim of this work, to determine the effect of host animal sex and sex hormones on bone formation mediated by MDSCs, was evaluated with an intramuscular ectopic bone formation model. Two hypotheses were tested: one, more MDSC-mediated intramuscular

ectopic bone formation would occur in male than in female host animals, and two castration and ovariectomy would not affect MDSC-mediated bone formation sex differences. Male hosts (whether unaltered or castrated) did form more bone than female hosts (whether unaltered or ovariectomized); bone formation rate was also significantly faster in male hosts. Castrated and ovariectomized hosts were not different from their unaltered same sex counterparts in bone volume or formation rate. Moreover, the new bone formed was comprised almost entirely of cells derived from the host animal. Differences in ectopic bone volume and formation rate were determined to be due to male hosts' accelerated turnover from cartilage to bone tissue during the endochondral ossification process mediated by retrovirally transduced MDSCs.

Ectopic bone formation assays are widely used as a first test of osteogenic therapies, but ectopic bone formation does not necessarily correlate with healing. Therefore, the second aim of this work, to determine the effect of host animal sex and sex hormones on bone healing mediated by MDSCs, was evaluated in a cranial defect model. Again, two hypotheses were tested: one MDSC-mediated cranial defect healing would be superior in male compared to female host animals, and two castration and ovariectomy would not affect MDSC-mediated bone healing sex differences. Like the first study, sex differences were seen (both males hosts versus both female hosts); however, differences in some measures, for example total bone volume, were found between hosts of the same sex (unaltered male and castrated male or unaltered female and ovariectomized female). Histological findings between host groups of the same sex were identical though, and most importantly, in all host groups, endochondral bone formation, not intramembranous healing was occurring at the defect site. As in the ectopic bone formation model, male hosts (both unaltered and castrated) displayed more rapid remodeling from cartilage to bone during the endochondral bone formation process when compared to female hosts (both

unaltered and ovariectomized). Although bone formed at the defect site in all host groups, it was not in the ideal spatial location; large volumes of endochondral bone formed in, adjacent to, and above the cranial defect site. Future studies to modulate this bone growth to a more desirable shape and location are needed. Other scaffolds could be explored, including a biomaterial in sheet form, like small intestinal submucosa. A scaffold that maintains the shape of the defect could be advantageous over the liquid nature of the fibrin sealant used in this study. An inducible retroviral vector for BMP could also prove beneficial [11, 16]; a tet-on system could provide better regulation of the BMP delivered to the host cells, and when BMP expression is ended, perhaps the endochondral bone formed could remodel into a more desirable shape. Previous work by our group showed that co-implantation of MDSCs retrovirally transduced with BMP4 and cells transduced with Noggin more allowed controlled in vivo bone growth in a critical sized cranial defect model [16], and this method could also be examined in the context of host sex and sex hormones on bone healing.

Because MDSCs have been shown to mediate bone healing when applied at the time of bone defect creation, their therapeutic utility when applied to an established non-healing bone defect was postulated. The goal of the third aim was to determine the effect of MDSCs when applied to an established non-healing bone defect, and the hypothesis was MDSCs, when applied to a fibrous tissue filled non-healing bone defect, would induce healing in a manner similar to MDSCs applied at the time of creation of the defect. First attempts at an atrophic femoral non-union in mice proved unsuccessful; therefore, a mouse cranial non-union model was used, and MDSCs were applied after the normal course of wound healing. It was determined that there was no difference between no treatment, delayed treatment with fibrin and delayed treatment with non-transduced MDSCs; all of these groups showed minimal bone healing and similar fibrous

tissue distribution in the defect. Animals that were treated with MDSC-B4 after the defect healed for three weeks did form new bone that covered the defect; however, this bone was formed through endochondral ossification, and fibrous tissue located in the defect was unaltered by MDSC-B4 application. Most importantly, application of MDSC-B4 to an established non-healing cranial defect did bring about bone formation, which covered, but did not fill, the cranial defect. Future studies could examine means to modify MDSC-mediated bone formation to change the location and manner of bone formation. Again, modifying the scaffold could prove beneficial, allowing the bone to grow in a more desirable location. Because the fibrous tissue filling the defect was unaffected by MDSC treatment, this fibrous tissue could also be a target of future studies. Improvement in surgical techniques or moving to a larger animal model would allow more complete debridement of this tissue. Targeting this fibrous tissue through biologic degradation or remodeling could also prove beneficial. Revisiting the long bone non-union model could also provide valuable insight for clinical orthopaedic applications of MDSCs.

By examining MDSC-bone formation and healing in various models, each representing different patient populations, bench to beside translation of MDSCs for clinical therapies moves closer. Differences by host sex, but not sex hormones, were found in MDSC-mediated ectopic bone formation, and differences by both host sex and sex hormone status were found when examining MDSCs as a treatment for cranial defects. MDSCs were also proven to be a viable treatment for established non-healing bone defects. The work presented here is a first step toward clinical translation of MDSCs for bone healing applications.

APPENDIX

ATTEMPT AT MODEL OF LONG BONE NON-UNION IN MICE

A.1 INTRODUCTION

Long bone non-unions present a significant challenge to orthopaedic surgeons. Currently, BMP protein therapies are sometimes applied to long bone non-unions [47-49], but perhaps MDSCs could provide another cellular source for non-union treatment. The purpose of this study was to establish an effective, reproducible mouse model of femoral non-union so that syngeneic mouse MDSCs could be applied to this defect and examined for efficacy. Several groups have attempted to develop a mouse femoral non-union model; however, this is a technically challenging model and results are controversial [111-114]. This study was funded by a grant

from The Albert B. Ferguson, Jr. M.D. Orthopaedic Fund of The Pittsburgh Foundation to PI Laura Meszaros.

The original experimental design was three branches: non-union with no treatment, non-union with MDSCs applied after non-union diagnosis has been established, and finally non-union model with MDSCs applied at time of creation of fracture in order to determine if MDSCs could prevent non-union formation. Foremost, a non-healing fracture model had to be established before treatments could be devised, and this model must be reproducible and create the desired effect (a non-healing femoral fracture). This appendix outlines an experiment aimed at establishing a non-union model; however, this pilot study was unsuccessful and therefore a critical-size cranial defect model was instead used to test MDSCs in a non-healing bone defect (Chapter 4.0).

A.2 METHODS

For mouse femoral non-union, C57BL/10J mice purchased from Jackson Laboratories were used. Surgeries were performed at age 8 weeks. Following sterile surgical procedures outlined in the University of Pittsburgh IACUC Protocol #090138, each animal was anesthetized and an incision was made along the patella. The patella was dislocated laterally and a 23G needle was used to drill through the distal femur. This pilot drill was then removed, and a second 23G needle was inserted as an intramedullary nail. This second needle was clipped to a length slightly shorter than the length of the femur and allowed to slide completely inside of the femur. The patella was relocated, and the parapatellar incision was closed with a suture. Next, an incision was made laterally along the femur. Through the intramuscular septum of the quadriceps, a

femoral fracture was made circumferentially with a small pair of scissors. A small cauterizer (Optitemp IIV) was then used on the periosteum along the edge of the fracture, circumferentially on both proximal and distal ends. Finally, the second incision was closed with sutures and the animals were allowed to resume normal activity. Animals were sacrificed at 7 weeks following surgery. This surgical procedure was a modification of the procedure outlined in Oetgen et al, but in contrast, the needle used as an intramedullary nail was inserted before any fracture or osteotomy was created.

A.3 RESULTS

One mouse died five days following the surgery; cause of death was unknown but upon examination was determined to not be due to pin migration, bleeding at fracture site or obvious infection.

It was intended that microCT scanning would be used for evaluation and quantification of healing of the fracture. However, the stainless steel pin used caused significant scatter artifact. Therefore, each animal remaining was assessed using the pilot scan function of the microCT, which is essentially a planar radiograph. All pins were located correctly (within the femur) in six animals; in two animals there was possible proximal pin migration, and in one animal there was possible distal pin migration.

Figure 31: Representative pilot microCT scan at 1 week post injury

At 7 weeks after fracture creation, all animals were evaluated using planar radiographs. A surgeon evaluated each radiograph and scored as healed, partially healed or open. Of the nine animals evaluated, four were determined to be radiographically healed, while two additional animals were partially healed. Only three animals were determined to have radiographic non-union at 7 weeks after fracture creation.

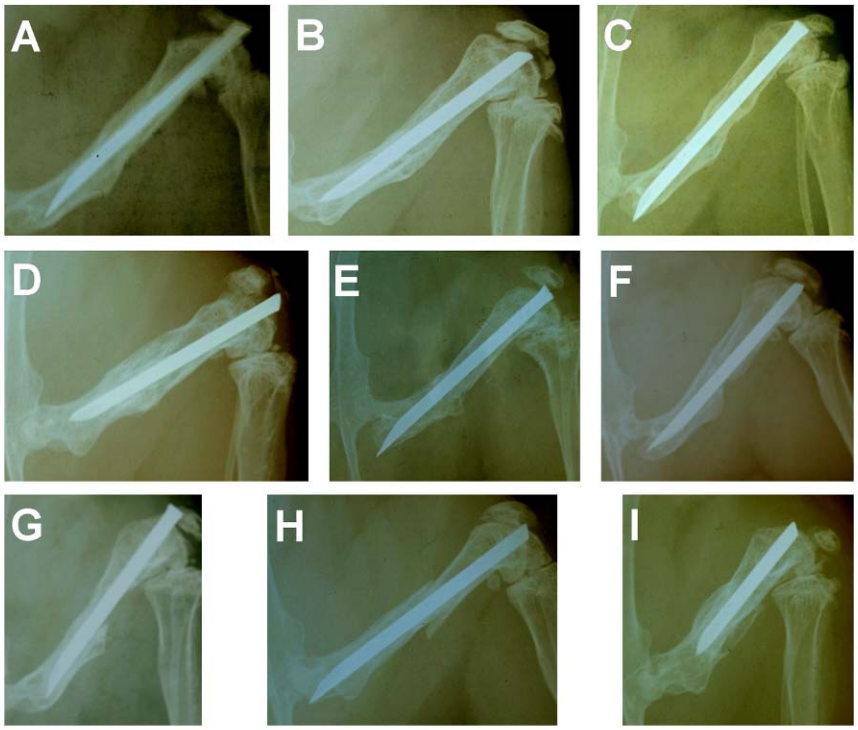

Figure 32: Radiographs of fracture healing at 7 weeks post injury

Radiographs of fracture healing of nine surviving mice at 7 weeks A) healed B) healed C) healed D) healed E) partially healed F) partially healed G) open H) open I) open

Because the model failed to give repeatable non-union of a mouse femoral fracture and only three of nine fractures remained open, this approach was discontinued and no further analyses (histological analysis, gait analysis, etc) were performed. Instead a non-healing critical size cranial defect was used to determine if MDSCs can induce repair in a non-healing bone defect.

A.4 DISCUSSION

This preliminary experiment was undertaken to determine a model of mouse femoral non-union. It was hoped that this model would then be used to test the efficacy MDSCs for treating an established non-union or preventing non-union occurrence in a recognized non-union model. Ten animals were used for a pilot study to perfect the model, and the purpose of this study was two-fold: one, to determine that this procedure, in fact, created a non-healing femoral defect, and two, that this procedure created a non-healing defect in all animals, i.e. it is repeatable.

Although this surgical procedure was performed by a surgeon, Dr. Yutaka Mifune, with experience in rat non-union and mouse fracture models [115-117], we were unable to recreate a femoral non-union model in mice. Two papers have been published, both in 2008, outlining a femoral non-union model in mice: Garcia et al and Oetgen et al [112, 114]. These papers use a similar method of creating the non-union (fracture with fixation and cauterization of periosteum), but the merits of each are debated [111-114]. Garcia et al outline a procedure with a small gauge needle as an intramedullary nail and a “custom-made clip”, which appears to be a surgical staple, as a fixation device. A bone defect gap of either .8 or 1.88mm was then created and the periosteum surrounding was removed or left undisturbed. Of all of these combinations, only the periosteum-stripped, 1.8mm defect resulted in non-union in all animals tested, and this was confirmed with histological and radiographic analyses [112]. This model was classified as an atrophic non-union. An attempt was made at recreating the fixation device in our laboratory, using surgical staples (Signet Autosuture) and a 23G needle as an intramedullary nail, on adult mice which were sacrificed for another experiment. These attempts were unsuccessful because even though the surgical staples we used appeared to be the same size as those used by Garcia et al, it was impossible to insert the pins into the thin cortical bone of the mouse femur without

either contacting the intramedullary nail or causing secondary fractures of the cortical bone at the insertion site. Due to these technical challenges, it was determined that this procedure outlined by Garcia et al was not a feasible surgical technique, and therefore, the method outlined by Oetgen et al was pursued.

Briefly, this method involves creating a partial osteotomy, inserting a needle as an intramedullary nail, then completing the fracture and cauterizing the periosteum [114]. A modified version of this protocol, eliminating the partial osteotomy step, was used in our pilot study. Several concerns have subsequently been raised about this study though. Lack of radiographic and statistical analyses are noted, as well as no description of infection or antibiotic administration [113]. This procedure is also criticized because it models a hypertrophic non-union, not an atrophic non-union, which some consider to be a more clinically important problem [111]. Regardless of critiques, in our laboratory, this method proved to be unsuccessful, with six of nine animals demonstrating partial or complete healing of the supposed non-union.

Although a reproducible mouse femoral non-union model would be a desirable experimental tool, this model is not without technical challenges. Standardized protocols for non-unions, as well as fracture healing models, must be established and adhered to if murine studies are used to test cellular or tissue engineered bone therapies [118]. Because a standardized long bone non-union protocol could not be established in our laboratory, a mouse non-healing cranial defect model was used instead to test MDSC therapies.

BIBLIOGRAPHY

1. Gharaibeh, B., et al., *Isolation of a slowly adhering cell fraction containing stem cells from murine skeletal muscle by the preplate technique.* Nat Protoc, 2008. **3**(9): p. 1501-9.

2. Jankowski, R.J., et al., *Flow cytometric characterization of myogenic cell populations obtained via the preplate technique: potential for rapid isolation of muscle-derived stem cells.* Hum Gene Ther, 2001. **12**(6): p. 619-28.

3. Lee, J.Y., et al., *Clonal isolation of muscle-derived cells capable of enhancing muscle regeneration and bone healing.* J Cell Biol, 2000. **150**(5): p. 1085-100.

4. Qu-Petersen, Z., et al., *Identification of a novel population of muscle stem cells in mice: potential for muscle regeneration.* J Cell Biol, 2002. **157**(5): p. 851-64.

5. Cao, B., et al., *Muscle stem cells differentiate into haematopoietic lineages but retain myogenic potential.* Nat Cell Biol, 2003. **5**(7): p. 640-6.

6. Kuroda, R., et al., *Cartilage repair using bone morphogenetic protein 4 and muscle-derived stem cells.* Arthritis Rheum, 2006. **54**(2): p. 433-42.

7. Peng, H., et al., *Synergistic enhancement of bone formation and healing by stem cell-expressed VEGF and bone morphogenetic protein-4.* J Clin Invest, 2002. **110**(6): p. 751-9.

8. Shen, H.C., et al., *Ex vivo gene therapy-induced endochondral bone formation: comparison of muscle-derived stem cells and different subpopulations of primary muscle-derived cells.* Bone, 2004. **34**(6): p. 982-92.

9. Wright, V., et al., *BMP4-expressing muscle-derived stem cells differentiate into osteogenic lineage and improve bone healing in immunocompetent mice.* Mol Ther, 2002. **6**(2): p. 169-78.

10. Musgrave, D.S., et al., *Ex vivo gene therapy to produce bone using different cell types.* Clin Orthop Relat Res, 2000(378): p. 290-305.

11. Peng, H., et al., *Development of a self-inactivating tet-on retroviral vector expressing bone morphogenetic protein 4 to achieve regulated bone formation.* Mol Ther, 2004. **9**(6): p. 885-94.

12. Shen, H.C., et al., *Structural and functional healing of critical-size segmental bone defects by transduced muscle-derived cells expressing BMP4.* J Gene Med, 2004. **6**(9): p. 984-91.

13. Musgrave, D.S., et al., *Human skeletal muscle cells in ex vivo gene therapy to deliver bone morphogenetic protein-2.* J Bone Joint Surg Br, 2002. **84**(1): p. 120-7.

14. Lee, J.Y., et al., *Enhancement of bone healing based on ex vivo gene therapy using human muscle-derived cells expressing bone morphogenetic protein 2.* Hum Gene Ther, 2002. **13**(10): p. 1201-11.

15. Hannallah, D., et al., *Retroviral delivery of Noggin inhibits the formation of heterotopic ossification induced by BMP-4, demineralized bone matrix, and trauma in an animal model.* J Bone Joint Surg Am, 2004. **86-A**(1): p. 80-91.

16. Peng, H., et al., *Noggin improves bone healing elicited by muscle stem cells expressing inducible BMP4.* Mol Ther, 2005. **12**(2): p. 239-46.

17. Peng, H., et al., *VEGF improves, whereas sFlt1 inhibits, BMP2-induced bone formation and bone healing through modulation of angiogenesis.* J Bone Miner Res, 2005. **20**(11): p. 2017-27.

18. Corsi, K.A., et al., *The Osteogenic Potential of Postnatal Skeletal Muscle-Derived Stem Cells is Influenced by Donor Sex.* J Bone Miner Res, 2007.

19. Deasy, B.M., et al., *A role for cell sex in stem cell-mediated skeletal muscle regeneration: female cells have higher muscle regeneration efficiency.* J Cell Biol, 2007. **177**(1): p. 73-86.

20. Matsumoto, T., et al., *The influence of sex on the chondrogenic potential of muscle-derived stem cells: implications for cartilage regeneration and repair.* Arthritis Rheum, 2008. **58**(12): p. 3809-19.

21. Payne, K.A., D.M. Didiano, and C.R. Chu, *Donor sex and age influence the chondrogenic potential of human femoral bone marrow stem cells.* Osteoarthritis Cartilage, 2010. **18**(5): p. 705-13.

22. Hoetzer, G.L., et al., *Gender differences in circulating endothelial progenitor cell colony-forming capacity and migratory activity in middle-aged adults.* Am J Cardiol, 2007. **99**(1): p. 46-8.

23. Crisostomo, P.R., et al., *In the adult mesenchymal stem cell population, source gender is a biologically relevant aspect of protective power.* Surgery, 2007. **142**(2): p. 215-21.

24. Ishida, Y. and J.N. Heersche, *Progesterone stimulates proliferation and differentiation of osteoprogenitor cells in bone cell populations derived from adult female but not from adult male rats.* Bone, 1997. **20**(1): p. 17-25.

25. Dudas, J.R., et al., *Leporine-derived adipose precursor cells exhibit in vitro osteogenic potential.* J Craniofac Surg, 2008. **19**(2): p. 360-8.

26. Ogawa, R., et al., *Adipogenic differentiation by adipose-derived stem cells harvested from GFP transgenic mice-including relationship of sex differences.* Biochem Biophys Res Commun, 2004. **319**(2): p. 511-7.

27. Seeman, E., *Clinical review 137: Sexual dimorphism in skeletal size, density, and strength.* J Clin Endocrinol Metab, 2001. **86**(10): p. 4576-84.

28. Nieves, J.W., et al., *Males have larger skeletal size and bone mass than females, despite comparable body size.* J Bone Miner Res, 2005. **20**(3): p. 529-35.

29. Tosi, L.L., B.D. Boyan, and A.L. Boskey, *Does sex matter in musculoskeletal health? The influence of sex and gender on musculoskeletal health.* J Bone Joint Surg Am, 2005. **87**(7): p. 1631-47.

30. Pinn, V.W., *Past and future: sex and gender in health research, the aging experience, and implications for musculoskeletal health.* Orthop Clin North Am, 2006. **37**(4): p. 513-21.

31. Csete, M., *Gender issues in transplantation.* Anesth Analg, 2008. **107**(1): p. 232-8.

32. Baratz, M., A.D. Watson, and J.E. Imbriglia, *Orthopaedic surgery : the essentials*. 1999, New York: Thieme. 23-28.

33. Rockwood, C.A., et al., *Rockwood and Green's fractures in adults*. 6th ed. 2006, Philadelphia, PA: Lippincott Williams & Wilkins. 2 v. (xvii, 2400, I-52).

34. Fischgrund, J.S., *Orthopaedic knowledge update 9*. 2007, Rosemont, Ill.
London: American Academy of Orthopaedic Surgeons ;
Eurospan distributor. xx, 840.

35. Tuan, R.S., *Biology of developmental and regenerative skeletogenesis.* Clin Orthop Relat Res, 2004(427 Suppl): p. S105-17.

36. USFDA, *Guidance Document for the Preparation of Investigational Device Exemptions and Pre-market Approval Applications for Bone Growth Stimulator Devices* 1988 United States Food and Drug Administration.

37. Frolke, J.P. and P. Patka, *Definition and classification of fracture non-unions.* Injury, 2007. **38 Suppl 2**: p. S19-22.

38. Obert, L., F. Deschaseaux, and P. Garbuio, *Critical analysis and efficacy of BMPs in long bones non-union.* Injury, 2005. **36 Suppl 3**: p. S38-42.

39. Panetta, N.J., et al., *Tissue Engineering in Cleft Palate and Other Congenital Malformations.* Pediatr Res, 2008.

40. Jones, C.B. and K.A. Mayo, *Nonunion treatment: iliac crest bone graft techniques.* J Orthop Trauma, 2005. **19**(10 Suppl): p. S11-3.

41. Sen, M.K. and T. Miclau, *Autologous iliac crest bone graft: should it still be the gold standard for treating nonunions?* Injury, 2007. **38 Suppl 1**: p. S75-80.

42. De Long, W.G., Jr., et al., *Bone grafts and bone graft substitutes in orthopaedic trauma surgery. A critical analysis.* J Bone Joint Surg Am, 2007. **89**(3): p. 649-58.

43. Smith, D.M., et al., *Bone morphogenetic protein 2 therapy for craniofacial surgery.* J Craniofac Surg, 2008. **19**(5): p. 1244-59.

44. Govender, S., et al., *Recombinant human bone morphogenetic protein-2 for treatment of open tibial fractures: a prospective, controlled, randomized study of four hundred and fifty patients.* J Bone Joint Surg Am, 2002. **84-A**(12): p. 2123-34.

45. McKay, W.F., S.M. Peckham, and J.M. Badura, *A comprehensive clinical review of recombinant human bone morphogenetic protein-2 (INFUSE Bone Graft).* Int Orthop, 2007. **31**(6): p. 729-34.

46. Swiontkowski, M.F., et al., *Recombinant human bone morphogenetic protein-2 in open tibial fractures. A subgroup analysis of data combined from two prospective randomized studies.* J Bone Joint Surg Am, 2006. **88**(6): p. 1258-65.

47. Crawford, C.H., 3rd and D. Seligson, *Atrophic nonunion of humeral diaphysis treated with locking plate and recombinant bone morphogenetic protein: nine cases.* Am J Orthop (Belle Mead NJ), 2009. **38**(11): p. 567-70.

48. Johnson, E.E. and M.R. Urist, *Human bone morphogenetic protein allografting for reconstruction of femoral nonunion.* Clin Orthop Relat Res, 2000(371): p. 61-74.

49. White, A.P., et al., *Clinical applications of BMP-7/OP-1 in fractures, nonunions and spinal fusion.* Int Orthop, 2007. **31**(6): p. 735-41.

50. Schmidmaier, G., et al., *Quantitative assessment of growth factors in reaming aspirate, iliac crest, and platelet preparation.* Bone, 2006. **39**(5): p. 1156-63.

51. Urist, M.R., *Bone: formation by autoinduction.* Science, 1965. **150**(698): p. 893-9.

52. Li, G., et al., *Differential effect of BMP4 on NIH/3T3 and C2C12 cells: implications for endochondral bone formation.* J Bone Miner Res, 2005. **20**(9): p. 1611-23.

53. Usas, A., et al., *Bone regeneration mediated by BMP4-expressing muscle-derived stem cells is affected by delivery system.* Tissue Eng Part A, 2009. **15**(2): p. 285-93.

54. Young, B.H., H. Peng, and J. Huard, *Muscle-based gene therapy and tissue engineering to improve bone healing.* Clin Orthop Relat Res, 2002(403 Suppl): p. S243-51.

55. Bergman, K., et al., *Injectable cell-free template for bone-tissue formation.* J Biomed Mater Res A, 2009. **91**(4): p. 1111-8.

56. Mauney, J.R., et al., *Matrix-mediated retention of in vitro osteogenic differentiation potential and in vivo bone-forming capacity by human adult bone marrow-derived mesenchymal stem cells during ex vivo expansion.* J Biomed Mater Res A, 2006. **79**(3): p. 464-75.

57. Musgrave, D.S., et al., *Adenovirus-mediated direct gene therapy with bone morphogenetic protein-2 produces bone.* Bone, 1999. **24**(6): p. 541-7.

58. Alden, T.D., et al., *In vivo endochondral bone formation using a bone morphogenetic protein 2 adenoviral vector.* Hum Gene Ther, 1999. **10**(13): p. 2245-53.

59. Schmitz, J.P. and J.O. Hollinger, *The critical size defect as an experimental model for craniomandibulofacial nonunions.* Clin Orthop Relat Res, 1986(205): p. 299-308.

60. Hollinger, J.O. and J.C. Kleinschmidt, *The critical size defect as an experimental model to test bone repair materials.* J Craniofac Surg, 1990. **1**(1): p. 60-8.

61. Gosain, A.K., et al., *Osteogenesis in cranial defects: reassessment of the concept of critical size and the expression of TGF-beta isoforms.* Plast Reconstr Surg, 2000. **106**(2): p. 360-71; discussion 372.

62. Cooper, G.M., et al., *Testing the critical size in calvarial bone defects: revisiting the concept of a critical-size defect.* Plast Reconstr Surg, 2010. **125**(6): p. 1685-92.

63. Lee, J.Y., et al., *Effect of bone morphogenetic protein-2-expressing muscle-derived cells on healing of critical-sized bone defects in mice.* J Bone Joint Surg Am, 2001. **83-A**(7): p. 1032-9.

64. Bhuiyan, S. and K. Fukunaga, *Stimulation of Sigma-1 receptor by dehydroepiandrosterone ameliorates hypertension-induced kidney hypertrophy in ovariectomized rats.* Exp Biol Med (Maywood), 2010. **235**(3): p. 356-64.

65. De la Fuente, M. and L. Gimenez-Llort, *Models of aging of neuroimmunomodulation: strategies for its improvement.* Neuroimmunomodulation, 2010. **17**(3): p. 213-6.

66. Fukuhara, S., S. Matsushita, and Y. Sakakibara, *Changes in coronary resistance related to the stages of the female life cycle.* Circ J, 2006. **70**(4): p. 478-81.

67. Liu, F., et al., *Changes in experimental stroke outcome across the life span.* J Cereb Blood Flow Metab, 2009. **29**(4): p. 792-802.

68. Fortepiani, L.A., et al., *Role of androgens in mediating renal injury in aging SHR.* Hypertension, 2003. **42**(5): p. 952-5.

69. Meyers, B., et al., *Gonadectomy and hormone replacement exert region- and enzyme isoform-specific effects on monoamine oxidase and catechol-O-methyltransferase activity in prefrontal cortex and neostriatum of adult male rats.* Neuroscience, 2010. **165**(3): p. 850-62.

70. Sosic-Jurjevic, B., et al., *Suppressive effects of genistein and daidzein on pituitary-thyroid axis in orchidectomized middle-aged rats.* Exp Biol Med (Maywood), 2010. **235**(5): p. 590-8.

71. Kalu, D.N., *The ovariectomized rat model of postmenopausal bone loss.* Bone Miner, 1991. **15**(3): p. 175-91.

72. Kalu, D.N., et al., *The aged rat model of ovarian hormone deficiency bone loss.* Endocrinology, 1989. **124**(1): p. 7-16.

73. Feher, A., et al., *Bisphosphonates do not inhibit periosteal bone formation in estrogen deficient animals and allow enhanced bone modeling in response to mechanical loading.* Bone, 2010. **46**(1): p. 203-7.

74. Sarban, S., et al., *Can rhBMP-2 containing collagen sponges enhance bone repair in ovariectomized rats?: a preliminary study.* Clin Orthop Relat Res, 2009. **467**(12): p. 3113-20.

75. Shahnazari, M., et al., *Diet calcium level but not calcium supplement particle size affects bone density and mechanical properties in ovariectomized rats.* J Nutr, 2009. **139**(7): p. 1308-14.

76. Almeida, M., et al., *Skeletal involution by age-associated oxidative stress and its acceleration by loss of sex steroids.* J Biol Chem, 2007. **282**(37): p. 27285-97.

77. Montero, M., et al., *The effectiveness of intermittent rat parathyroid hormone (1-34) treatment on low bone mass due to oestrogen or androgen depletion in skeletally mature rats.* Aging Male, 2010. **13**(1): p. 59-73.

78. Proell, V., et al., *Orchiectomy upregulates free soluble RANKL in bone marrow of aged rats.* Bone, 2009. **45**(4): p. 677-81.

79. Peng, H., et al., *Development of an MFG-based retroviral vector system for secretion of high levels of functionally active human BMP4.* Mol Ther, 2001. **4**(2): p. 95-104.

80. Burnett, C.C. and A.H. Reddi, *Influence of estrogen and progesterone on matrix-induced endochondral bone formation.* Calcif Tissue Int, 1983. **35**(4-5): p. 609-14.

81. Kapur, S.P. and A.H. Reddi, *Influence of testosterone and dihydrotestosterone on bone-matrix induced endochondral bone formation.* Calcif Tissue Int, 1989. **44**(2): p. 108-13.

82. McMillan, J., et al., *Osteoinductivity of demineralized bone matrix in immunocompromised mice and rats is decreased by ovariectomy and restored by estrogen replacement.* Bone, 2007. **40**(1): p. 111-21.

83. Bouxsein, M.L., et al., *Ovariectomy-induced bone loss varies among inbred strains of mice.* J Bone Miner Res, 2005. **20**(7): p. 1085-92.

84. Zhang, Y., et al., *Short- to mid-term effects of ovariectomy on bone turnover, bone mass and bone strength in rats.* Biol Pharm Bull, 2007. **30**(5): p. 898-903.

85. Coxam, V., et al., *Effects of dihydrotestosterone alone and combined with estrogen on bone mineral density, bone growth, and formation rates in ovariectomized rats.* Bone, 1996. **19**(2): p. 107-14.

86. Boyd, S.K., et al., *Monitoring individual morphological changes over time in ovariectomized rats by in vivo micro-computed tomography.* Bone, 2006. **39**(4): p. 854-62.

87. Klinck, J. and S.K. Boyd, *The magnitude and rate of bone loss in ovariectomized mice differs among inbred strains as determined by longitudinal in vivo micro-computed tomography.* Calcif Tissue Int, 2008. **83**(1): p. 70-9.

88. Govoni, K.E., et al., *Prepubertal OVX increases IGF-I expression and bone accretion in C57BL/6J mice.* Am J Physiol Endocrinol Metab, 2008. **295**(5): p. E1172-80.

89. Riggs, B.L., S. Khosla, and L.J. Melton, 3rd, *Sex steroids and the construction and conservation of the adult skeleton.* Endocr Rev, 2002. **23**(3): p. 279-302.

90. Vanderschueren, D., et al., *Androgens and bone.* Endocr Rev, 2004. **25**(3): p. 389-425.

91. Abu, E.O., et al., *The localization of androgen receptors in human bone.* J Clin Endocrinol Metab, 1997. **82**(10): p. 3493-7.

92. Crisan, M., et al., *A perivascular origin for mesenchymal stem cells in multiple human organs.* Cell Stem Cell, 2008. **3**(3): p. 301-13.

93. Dellavalle, A., et al., *Pericytes of human skeletal muscle are myogenic precursors distinct from satellite cells.* Nat Cell Biol, 2007. **9**(3): p. 255-67.

94. Zheng, B., et al., *Prospective identification of myogenic endothelial cells in human skeletal muscle.* Nat Biotechnol, 2007. **25**(9): p. 1025-34.

95. Lounev, V.Y., et al., *Identification of progenitor cells that contribute to heterotopic skeletogenesis.* J Bone Joint Surg Am, 2009. **91**(3): p. 652-63.

96. Kobori, M. and T. Yamamuro, *Effects of gonadectomy and estrogen administration on rat skeletal muscle.* Clin Orthop Relat Res, 1989(243): p. 306-11.

97. McCormick, K.M., et al., *Effects of ovariectomy and estrogen on skeletal muscle function in growing rats.* J Muscle Res Cell Motil, 2004. **25**(1): p. 21-7.

98. Yang, X., et al., *Tissue-specific expression and regulation of sexually dimorphic genes in mice.* Genome Res, 2006. **16**(8): p. 995-1004.

99. Clancy, B.M., et al., *A gene expression profile for endochondral bone formation: oligonucleotide microarrays establish novel connections between known genes and BMP-2-induced bone formation in mouse quadriceps.* Bone, 2003. **33**(1): p. 46-63.

100. Beil, F.T., et al., *Effects of Increased Bone Formation on Fracture Healing in Mice.* J Trauma, 2010

101. Peng, H., et al., *Converse relationship between in vitro osteogenic differentiation and in vivo bone healing elicited by different populations of muscle-derived cells genetically engineered to express BMP4.* J Bone Miner Res, 2004. **19**(4): p. 630-41.

102. Chang, M.A., et al., *The outcomes and complications of 1,2-intercompartmental supraretinacular artery pedicled vascularized bone grafting of scaphoid nonunions.* J Hand Surg Am, 2006. **31**(3): p. 387-96.

103. Li, Z., et al., *Abnormal union of mandibular fractures: a review of 84 cases.* J Oral Maxillofac Surg, 2006. **64**(8): p. 1225-31.

104. Parker, M.J., R. Raghavan, and K. Gurusamy, *Incidence of fracture-healing complications after femoral neck fractures.* Clin Orthop Relat Res, 2007. **458**: p. 175-9.

105. Melhus, G., et al., *Experimental osteoporosis induced by ovariectomy and vitamin D deficiency does not markedly affect fracture healing in rats.* Acta Orthop, 2007. **78**(3): p. 393-403.

106. Hao, Y.J., et al., *Changes of microstructure and mineralized tissue in the middle and late phase of osteoporotic fracture healing in rats.* Bone, 2007. **41**(4): p. 631-8.

107. Mehta, M., et al., *A 5-mm femoral defect in female but not in male rats leads to a reproducible atrophic non-union.* Arch Orthop Trauma Surg, 2010.

108. Strube, P., et al., *Sex-specific compromised bone healing in female rats might be associated with a decrease in mesenchymal stem cell quantity.* Bone, 2009. **45**(6): p. 1065-72.

109. Cooper, G.M., et al., *Inkjet-based biopatterning of bone morphogenetic protein-2 to spatially control calvarial bone formation.* Tissue Eng Part A, 2010. **16**(5): p. 1749-59.

110. Hirata, K., et al., *Transplantation of skin fibroblasts expressing BMP-2 promotes bone repair more effectively than those expressing Runx2.* Bone, 2003. **32**(5): p. 502-12.

111. Garcia, P., et al., *Femoral non-union models in the mouse.* Injury, 2010. **41**(7): p. 1058-9.

112. Garcia, P., et al., *Development of a reliable non-union model in mice.* J Surg Res, 2008. **147**(1): p. 84-91.

113. Memisoglu, K. and C.C. Kesemenli, *Re: Development of a femoral non-union model in the mouse.* Injury, 2009. **40**(4): p. 467.

114. Oetgen, M.E., et al., *Development of a femoral non-union model in the mouse.* Injury, 2008. **39**(10): p. 1119-26.

115. Matsumoto, T., et al., *Therapeutic potential of vasculogenesis and osteogenesis promoted by peripheral blood CD34-positive cells for functional bone healing.* Am J Pathol, 2006. **169**(4): p. 1440-57.

116. Matsumoto, T., et al., *Fracture induced mobilization and incorporation of bone marrow-derived endothelial progenitor cells for bone healing.* J Cell Physiol, 2008. **215**(1): p. 234-42.

117. Mifune, Y., et al., *Local delivery of granulocyte colony stimulating factor-mobilized CD34-positive progenitor cells using bioscaffold for modality of unhealing bone fracture.* Stem Cells, 2008. **26**(6): p. 1395-405.

118. Holstein, J.H., et al., *Advances in the establishment of defined mouse models for the study of fracture healing and bone regeneration.* J Orthop Trauma, 2009. **23**(5 Suppl): p. S31-8.